

# Oxidative Dehalogenation of Perhalogenated Benzenes by Cytochrome P450 Compound I<sup>†</sup>

John C Hackett,<sup>‡</sup> Toby T. Sanan, and Christopher M. Hadad\*

Department of Chemistry, The Ohio State University, 100 West 18th Avenue, Columbus, Ohio 43210

Received February 21, 2007; Revised Manuscript Received March 15, 2007

**ABSTRACT:** Resolution of the identity PBE (RI-PBE) and B3LYP density functional theory calculations are used to understand the cytochrome P450-catalyzed, Compound I-mediated oxidation of perchlorobenzenes, perfluorobenzenes, their phenols, and mixed chlorofluorobenzenes to form benzoquinones. Addition of Compound I to the chlorine-bearing carbon of perchlorobenzenes and perchlorophenols results in an apparently barrierless 1,2-shift of the chlorine atom to form hexachlorocyclohexadienones and hydroxypentachlorocyclohexadienones, respectively. Hexachlorocyclohexadienone has a significant electron affinity, and its radical anion expels chloride in a facile manner to give the pentachlorophenoxyl radical. Deprotonation of hydroxypentachlorocyclohexadienones results in the expulsion of chloride and provides a direct route to the production of tetrachloroquinones. Barrier heights for Compound I addition to fluorine-bearing carbons of hexafluorobenzene and pentafluorophenol are comparable to those computed for oxidation of benzene via an analogous reaction path. In contrast to the chlorinated cases, fluorine migration to cyclohexadienones occurs with a moderate barrier. Additionally, gas-phase elimination of fluoride from the hexafluorocyclohexadienone radical anion and deprotonated hydroxypentafluorocyclohexadienone are not facile. Rather, consideration of implicit and explicit solvent is required to achieve favorable thermochemistry for fluoride elimination and generation of the experimentally observed products. Finally, the theoretical approach described herein is predictive of the experimentally observed preferential elimination of fluorine from chloropentafluorobenzene and 1,3,5-trichloro-2,4,6-trifluorobenzene. These studies illustrate the effectiveness of P450 Compound I as an oxidant of halogenated aromatic hydrocarbons, which are persistent environmental contaminants, and the potential utility of such computational methods for predicting P450 metabolism.

Polyhalogenated aromatic compounds are persistent, hazardous environmental pollutants (1, 2). Partially chlorinated benzenes, biphenyls, and dioxins are degradable by some organisms (3–6). In contrast, more extensively halogenated species are degraded at very slow rates (7). Many enzymes require an unhalogenated carbon atom within the aromatic compound for it to be accepted as a substrate. Therefore, aerobic metabolism is inaccessible for perhalogenated species via many enzymatic pathways. The alternative is slower, reductive metabolism in anaerobic environments (8).

The cytochrome P450 enzymes have demonstrated the potential to oxidatively dehalogenate hydrocarbons including halogenated benzenes. Significant progress has been made in the protein engineering arena with the goal to develop bacterial P450 enzymes with enhanced dehalogenation kinetics for application in environmental bioremediation (9–16). Additionally, these enzymes play an important role in the bioactivation of halogenated benzenes. P450-catalyzed oxidative dehalogenation results in the formation of their corresponding arene oxides and benzoquinones (Scheme 1). Such intermediates can rapidly arylate cellular macromolecules, and benzoquinones may redox cycle to generate reactive oxygen species (17). We have been particularly interested in the chemistry of these reactive oxygen species (18).

The mechanism for P450-catalyzed oxidative dehalogenation of aromatic substrates has been extensively debated (17). A number of experimental studies have attempted to address this question; however, the primary oxidation products have never been directly identified because of their high reactivity toward covalent modification by proteins or by rapid reduction from soluble cofactors such as NADPH. The observed metabolites of microsomal P450 metabolism of hexachlorobenzene are pentachlorophenol and tetrachlorohydroquinone (Scheme 2). At low O<sub>2</sub> concentrations, no pentachlorobenzene, pentachlorophenol, or covalent binding

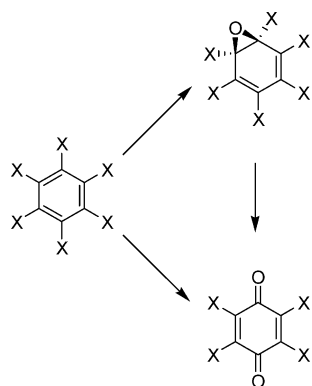
<sup>†</sup> This work was supported by the NSF-funded Environmental Molecular Science Institute (CHE-0089147) and The Ohio State University.

\* To whom correspondence should be addressed. Tel: (614) 688-3141. Fax: (614) 292-1685. E-mail: hadad.1@osu.edu.

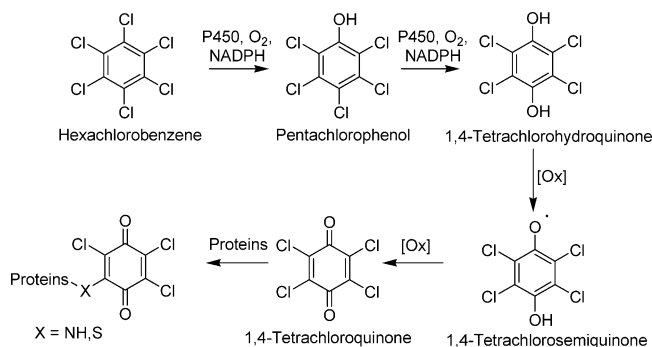
<sup>‡</sup> Current address: Department of Medicinal Chemistry and ISBDD, School of Pharmacy, Virginia Commonwealth University-MCV Campus, P.O. Box 980133, Richmond, VA 23219.

<sup>1</sup> Abbreviations: CYP2B1, cytochrome P450 2B1; GGA, generalized gradient approximation; ISP, infinitely separated products; ISR, infinitely separated reactants; mCPBA, *meta*-chloroperoxybenzoic acid; NADH, dihydronicotinamide adenine dinucleotide; NADPH, dihydronicotinamide adenine dinucleotide phosphate; NPA, natural population analysis; PCM, polarizable continuum model; PRC, pre-reactant complex; QM/MM, quantum mechanics/molecular mechanics; SORCI, spectroscopy oriented configuration interaction; TS, transition state; UCCSD(T), unrestricted coupled cluster theory with single and double excitations and non-iterative triple excitations.

Scheme 1



Scheme 2



to protein is detected. These results emphasize the relationship between protein binding and the microsomal oxidation of hexachlorobenzene. Tetrachlorohydroquinone is the primary metabolite detected after pentachlorophenol metabolism, which is in redox equilibrium with the corresponding semiquinone and quinone. Protein covalent binding is inhibited by the presence of ascorbic acid or glutathione in the incubations, supporting the involvement of a quinone species (Scheme 2) (19–21).

Experimental evidence suggests that the primary oxidation products of perhalogenated benzenes are tetrahaloquinones. P450-dependent monooxygenation at the fluorinated para position of anilines results in the release of fluoride and the reactive benzoquinoneimine as the primary reaction products (22). The oxidation of 2,3,5,6-tetrafluorophenol to tetrafluorohydroquinone is supported by NADPH and artificial oxygen donors, such as iodosobenzene and cumene hydroperoxide. In contrast, the conversion of pentafluorophenol to tetrafluorohydroquinone is only supported by NADPH. If cumene hydroperoxide or iodosobenzene are used as oxygen donors, addition of NADH is required to complete the transformation to tetrafluorohydroquinone. These studies suggest that pentafluorophenol is oxidized to a reactive species that can be reduced enzymatically or nonenzymatically with NAD(P)H. Taken together with the product results from the *para*-fluoroaniline studies, this reactive species has been suggested to be the tetrafluoroquinone, which has been demonstrated to rapidly modify microsomal proteins in a covalent fashion (23).

Direct halogen oxidation followed by hypohalous acid (HOX) elimination and phenol formation as the result of water addition has been proposed. However, this mechanistic possibility was eliminated for chlorine and fluorine substituents because no  $^{18}\text{O}$  label from  $^{18}\text{O}$   $\text{H}_2\text{O}$  was incorporated

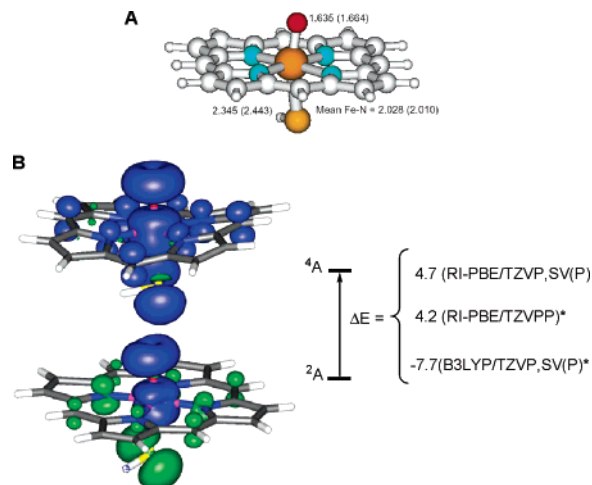


FIGURE 1: (A) RI-PBE/TZVP,SV(P) fully optimized geometry of the [(Porphyrin)(Fe=O)(SH)]<sup>0</sup> model of P450 Compound I used in this study. Key bond distances are listed in Angstroms. Values for the quartet state are in parentheses. (B) Spin difference density contours and doublet–quartet energetic splittings (kcal/mol) of the Compound I model. Blue contours correspond to an excess of  $\alpha$  spin density, whereas green contours correspond to an excess of  $\beta$  spin density. (\*) indicates single-point energies at the RI-PBE/TZVP,SV(P) geometry.

into pentachlorophenol formed from hexachlorobenzene oxidation (19).

Chemical models for P450 catalysis have been used to study the oxidative dehalogenation of substituted phenols. Ohe and co-workers used a *meso*-tetrakis(2,6-difluorophenyl)porphyrinatoiron(III) chloride with mCPBA as the oxygen donor. With this model system, halogens were eliminated with an efficiency trend of  $\text{F} > \text{Cl} > \text{Br}$ , and furthermore,  $^{18}\text{O}$  from  $^{18}\text{O}$  mCPBA was incorporated into the benzoquinones (24). The dehalogenation rates of perhalogenated anilines by the CYP2B1 isoenzyme occur with the same trend. Additionally, the same reactivity order is observed with dehalogenation by microperoxidase-8, which lacks an active site. These results indicate the rate of dehalogenation is dependent on the intrinsic electronic properties of the halogen substituents (22).

In this article, the oxidative dehalogenation mechanisms of a variety of perchlorinated and perfluorinated benzenes, their phenols, and mixed fluorinated/chlorinated benzenes are studied using a truncated model of cytochrome P450 Compound I and density functional theory. We locate transition states and intermediates for mechanistic proposals consistent with the available experimental data. The computational results described herein provide insight into the structure and reactivity of novel intermediates in the oxidative dehalogenation of perhalogenated aromatic compounds. Additionally, important mechanistic differences in the oxidative dehalogenation of chlorinated and fluorinated compounds are elucidated.

## COMPUTATIONAL METHODOLOGY

**Model System.** Compound I of cytochrome P450 was modeled as a [(Porphyrin)(Fe=O)(SH)]<sup>0</sup> complex (Figure 1A). QM/MM investigations by Schöneboom and co-workers, which included the full protoporphyrin IX and steric and electric field contributions of the surrounding apoprotein, revealed that this system could be a reliable

mimic for computationally intensive mechanistic studies (25). We have utilized this model earlier for a theoretical analysis of the final catalytic step of the aromatase P450 enzyme (26).

**Theoretical Methods.** Potential energy surfaces for the oxidation of perhalobenzenes by model Compound I were performed with the TURBOMOLE 5.71 suite of programs for electronic structure calculations (27–30). Geometry optimizations were performed using the Perdew, Burke, and Erzenhof density functional (31, 32) with the resolution of the identity approximation for computing the electronic Coulomb interaction (RI-PBE) (33–35). PBE, similar to other pure GGA functionals, has a tendency to disfavor high spin states compared to meta-GGA and hybrid density functionals; however, PBE was recently demonstrated to predict the relative spin state energetics for several iron complexes (36). The TZVP basis set for iron and the SV(P) basis sets for the remaining atoms were employed in all of the geometry optimizations (37, 38). Basis set effects were evaluated with single-point energy calculations using the TZVPP basis set for all atoms. Single-point energy calculations with the hybrid B3LYP density functional (39–43) with the TZVP and SV(P) basis sets were performed to assess the contribution of exact exchange to the computed properties, and furthermore, these results can be compared with previous calculations performed with this functional.

Calculations of isolated halobenzenes and their P450-catalyzed oxidation products were performed with the B3LYP functional and the 6-31G(d) basis set in the Gaussian03 suite of programs (44). Single-point energy calculations were performed with the aug-cc-pVTZ basis set. The effect of solvation on the electronic structure of these systems and their relative energetics were evaluated with the polarizable continuum model (PCM) of Tomasi and co-workers (45–49). Spherical harmonic (5d, 7f) basis functions were used in all calculations. Minima were verified to have all real vibrational frequencies (50). In TURBOMOLE, transition states were located using the program STATPT and verified to have a single imaginary vibrational frequency. These frequency analyses also provided the necessary parameters to compute zero-point vibrational energy and thermochemical corrections. These corrections were unscaled. Transition states were verified to connect appropriate minima on their potential energy surfaces by distorting the geometries along the normal modes associated with their imaginary vibrational frequencies and subsequently re-optimizing the geometries.

Population analyses were carried out with the natural population analysis (NPA) method (51) in the Gaussian03 suite of programs.

## RESULTS AND DISCUSSION

**Electronic Structure of P450 Compound I.** The pure density functional theory characteristics of the PBE functional allow for the application of the resolution-of-the-identity approximation for the electronic Coulomb interaction (RI-PBE). This approach allows us to treat relatively large models of enzyme active sites with significant improvements in computational efficiency. To our knowledge, there is no previous application of the RI-PBE method to models of P450 Compound I in the literature. In the past, these systems have been studied with the hybrid density functional B3LYP. Schöneboom and co-workers have calibrated the B3LYP spin

state energetics of further truncated models of P450 Compound I models against the multireference configuration interaction results. In this impressive work, a complete active space SORCI (52) and UCCSD(T) wavefunctions for triplet and quintet  $[\text{FeO}(\text{NH}_3)_4(\text{H}_2\text{O})]^{2+}$  were computed to be within 0.1–0.2 eV (53). We also considered these states of  $[\text{FeO}(\text{NH}_3)_4(\text{H}_2\text{O})]^{2+}$  at the RI-PBE and B3LYP levels of theory. RI-PBE predicts an energetic spacing of 0.53 eV; however, single-point energy calculations with the B3LYP functional predict a spacing of 0.15 eV, in excellent agreement with the *ab initio* results. B3LYP calculations with truncated models of Compound I alone or embedded in a P450 protein as part of a QM/MM study predicted that this species has two closely lying spin states. We are unaware of any experimental evidence validating the degeneracy of Compound I spin states in cytochrome P450 enzymes. These models predict each state having two electrons in a triplet configuration localized to the FeO moiety, while a third electron resides in an orbital of mixed porphyrin  $\pi$  and sulfur p character from the distal thiolate ligand. Antiferromagnetic and ferromagnetic coupling of the third electron to the FeO pair gives rise to doublet and quartet spin states (54–59). The geometries for the doublet and quartet states, spin difference density contour plots, and the doublet–quartet energy splittings computed with the RI-PBE method are shown in Figure 1. Geometric parameters for the model Compound I species are in agreement within the estimated experimental uncertainty in the crystal structure of oxyferrous cytochrome P450cam (60). RI-PBE predicts an electron density distribution similar to that of B3LYP. This similarity is illustrated in Figure 1, where blue contours correspond to an excess of  $\alpha$  spin density, whereas green contours correspond to an excess of  $\beta$  spin density. The contour surfaces of both spin states are consistent with an excess of parallel spin density localized to the FeO unit. In the doublet state, an excess of antiparallel spin density is localized on the porphyrin ring and on the sulfur of the thiolate ligand. In contrast, the contour surface of the quartet state displays an excess of parallel spin density localized on the porphyrin and sulfur of the thiolate ligand. These results are consistent with the triradicaloid electronic structure of Compound I computed at the B3LYP level of theory and validate the application of this efficient computational method to study the reactivity of Compound I.

**Oxidation of Hexachlorobenzene and Pentachlorophenol.** The energetics for the oxidation of hexachlorobenzene and all positions of pentachlorophenol are listed in Table 1. Potential energy surfaces and RI-PBE/TZVPP//RI-PBE/TZVP,SV(P) and B3LYP/TZVP,SV(P)//RI-PBE/TZVP,SV(P) energetics for Compound I addition to hexachlorobenzene and the para position of pentachlorophenol are shown in Figures 2 and 3, respectively. RI-PBE barriers for the oxidation of hexachlorobenzene by the Compound I model are 15.2–17.1 kcal/mol on the doublet surface and 15.1–16.6 kcal/mol on the quartet surface. The B3LYP values are somewhat higher on both spin surfaces, with computed barriers of 20.3 and 19.8 kcal/mol on the doublet and quartet surfaces, respectively. For comparison, we computed the barrier for Compound I addition to benzene. Barrier heights on the doublet surface at the RI-PBE level of theory were 11.2 to 11.8 kcal/mol for this process. B3LYP/TZVP,SV(P) single-point energies with these geometries



Table 1: Energies (kcal/mol) Relative to the Pre-Reactant Complex on the Doublet Surface for Oxidation of Hexachlorobenzene and Pentachlorophenol<sup>a,b</sup>

theory	ISR	PRC	TS	PC	ISP
hexachlorobenzene					
RI-PBE/TZVP,SV(P)	4.9 (5.5)	0.0 (4.2)	15.2 (15.1)	-22.5 (-13.8)	-12.3 (-10.1)
RI-PBE/TZVP,SV(P) + ZPE	4.6 (5.4)	0.0 (3.7)	14.6 (14.6)	-22.0 (-13.7)	-12.2 (-10.3)
RI-PBE/TZVPP	2.1 (2.2)	0.0 (4.1)	17.1 (16.6)	-18.0 (-10.5)	-14.9 (-12.8)
B3LYP/ TZVP,SV(P)	11.1 (3.0)	0.0 (0.5)	20.3 (19.8)	NC (NC)	-28.5 (-31.7)
<i>p</i> -pentachlorophenol					
RI-PBE/TZVP,SV(P)	4.5 (5.4)	0.0 (3.9)	14.0 (14.8)	-23.6 (-14.8)	-13.9 (-11.5)
RI-PBE/TZVP,SV(P) + ZPE	4.4 (5.1)	0.0 (3.7)	13.4 (14.1)	-23.0 (-15.0)	-13.7 (-11.7)
RI-PBE/TZVPP	1.7 (2.0)	0.0 (4.0)	15.8 (16.0)	-18.9 (-11.9)	-16.4 (-14.2)
B3LYP/ TZVP,SV(P)	10.7 (2.9)	0.0 (0.2)	19.2 (19.3)	-31.1 (-17.6)	-30.4 (-33.2)
<i>o</i> -pentachlorophenol <sup>b</sup>					
RI-PBE/TZVP,SV(P)	4.8 (13.8)	0.0 (-4.2)	14.6 (22.9)	-30.1 (-8.0)	-18.0 (-7.4)
RI-PBE/TZVP,SV(P) + ZPE	4.6 (14.4)	0.0 (-5.3)	13.9 (23.1)	-29.3 (-7.4)	-17.8 (-6.7)
RI-PBE/TZVPP	1.8 (8.1)	0.0 (-2.0)	16.2 (22.0)	-19.1 (-7.0)	-20.4 (-12.2)
B3LYP/ TZVP,SV(P)	11.0 (9.5)	0.0 (-6.2)	19.5 (39.6)	-29.4 (-11.3)	-33.7 (-30.2)
<i>m</i> -pentachlorophenol					
RI-PBE/TZVP,SV(P)	12.3 (5.0)	0.0 (12.0)	22.9 (14.8)	-18.7 (-15.0)	-6.0 (-11.6)
RI-PBE/TZVP,SV(P) + ZPE	12.5 (4.9)	0.0 (12.0)	22.8 (14.5)	-17.6 (-14.7)	-5.4 (-11.8)
RI-PBE/TZVPP	6.8 (1.8)	0.0 (9.2)	22.3 (16.5)	-17.0 (-11.4)	-10.8 (-13.8)
B3LYP/ TZVP,SV(P)	18.1 (2.7)	0.0 (7.8)	27.7 (19.8)	-28.3 (-17.4)	-22.1 (-32.6)
<i>ipso</i> -pentachlorophenol					
RI-PBE/TZVP,SV(P)	12.1 (5.8)	0.0 (11.1)	19.2 (12.0)	8.9 (-0.9)	9.9 (5.2)
RI-PBE/TZVP,SV(P) + ZPE	11.2 (5.7)	0.0 (9.9)	17.5 (11.6)	7.8 (-0.8)	9.0 (4.8)
RI-PBE/TZVPP	7.3 (2.1)	0.0 (9.5)	20.2 (13.9)	11.0 (2.8)	5.4 (2.1)
B3LYP/ TZVP,SV(P)	18.5 (0.0)	0.0 (7.4)	22.9 (16.0)	7.6 (-1.7)	-3.0 (-13.1)

<sup>a</sup> ISR = infinitely separated reactants, PRC = pre-reactant complex, TS = transition state, and ISP = infinitely separated products. The quartet energetics are listed in parentheses. NC = unconverged SCF. <sup>b</sup> The inverted doublet–quartet energy spacing in the PRC arises from an apparent phenol–Compound I hydrogen bond not present in the doublet PRC.

yielded a somewhat higher barrier of 15.3 kcal/mol for benzene oxidation. This value is comparable to that computed by others for the barrier to formation of the cationic  $\sigma$  complex of benzene and Compound I (57, 61, 69).

RI-PBE barriers for the oxidation of pentachlorophenol at the para position are slightly lower than those computed for hexachlorobenzene oxidation, with computed barriers of 14.0–15.8 kcal/mol and 14.8–16.0 kcal/mol on the doublet and quartet surfaces, respectively. On the doublet surface, barriers for the oxidation of pentachlorophenol at the ortho position are similar to those computed for para oxidation. These results are consistent with the detection of both tetrachloro-1,2-quinone and tetrachloro-1,4-quinone in P450 metabolism studies of pentachlorophenol and for which the 1,4-isomer is the dominant product. The ratio of the 1,4-isomer to the 1,2-isomer in these experiments varied depending on which P450 enzyme was catalyzing the reaction (20). Because the calculations do not reveal any energetic differences in the propensity for oxidation at either the ortho or para positions, it seems that the experimental predominance of the 1,4-isomer is related to orientational preferences of the substrate which is governed by the P450 active site residues. In contrast to the doublet surface, barriers for ortho oxidation on the quartet spin surface are significantly higher (22.0–23.1 kcal/mol at the RI-PBE level of theory and 39.6 kcal/mol at the B3LYP level of theory). These barriers arise from the increased stability of the pre-reactant complex relative to the transition state as the result of an apparent phenol–Compound I hydrogen bond.

The RI-PBE computed barriers of 22.3–22.9 kcal/mol and 27.7 kcal/mol at the B3LYP level of theory for meta oxidation are significantly higher than those for ortho or para oxidation. The barriers for oxidation on the quartet surface

are lower and comparable to those computed for hexachlorobenzene and the para oxidation of pentachlorophenol. However, the increased quartet–doublet energy spacing indicates that the high-spin surface may be inaccessible. Taken together, these results are consistent with the experimental absence of meta oxidation products in the P450-catalyzed oxidation of perchlorobenzenes.

The addition of Compound I to the ipso position of pentachlorophenol was also considered. With the exception of meta addition to pentachlorophenol, the computed barriers are 2.9–4.8 kcal/mol higher on the doublet surface, which is energetically preferred. Additionally, this process is endothermic on the doublet surface and nearly thermoneutral on the quartet surface. It is likely that if the phenolic hydroxyl group oriented itself in the enzyme active site poised for ipso addition, the oxidation pathway would be required to compete with an energetically facile proton or hydrogen-atom abstraction process, and ipso attack is unlikely to contribute to the oxidation of this compound.

Important geometric parameters, group spin densities and atomic charges for intermediates and transition states on the potential energy surfaces for hexachlorobenzene and para oxidation of pentachlorophenol are shown in Figures 2 and 3. The results for oxidation at other positions on pentachlorophenol are qualitatively similar; therefore, these data are provided in the Supporting Information. The reaction proceeds with an early transition state consistent with their relative energetic similarity to the pre-reactant complexes. In this transition state, the oxygen of Compound I approaches hexachlorobenzene at an angle of 107° (62) with a C–O distance of 1.8 Å. The calculated angles in these transition states are similar to the approach angle of 105° described by Bürgi and Dunitz for the nucleophilic addition of amines

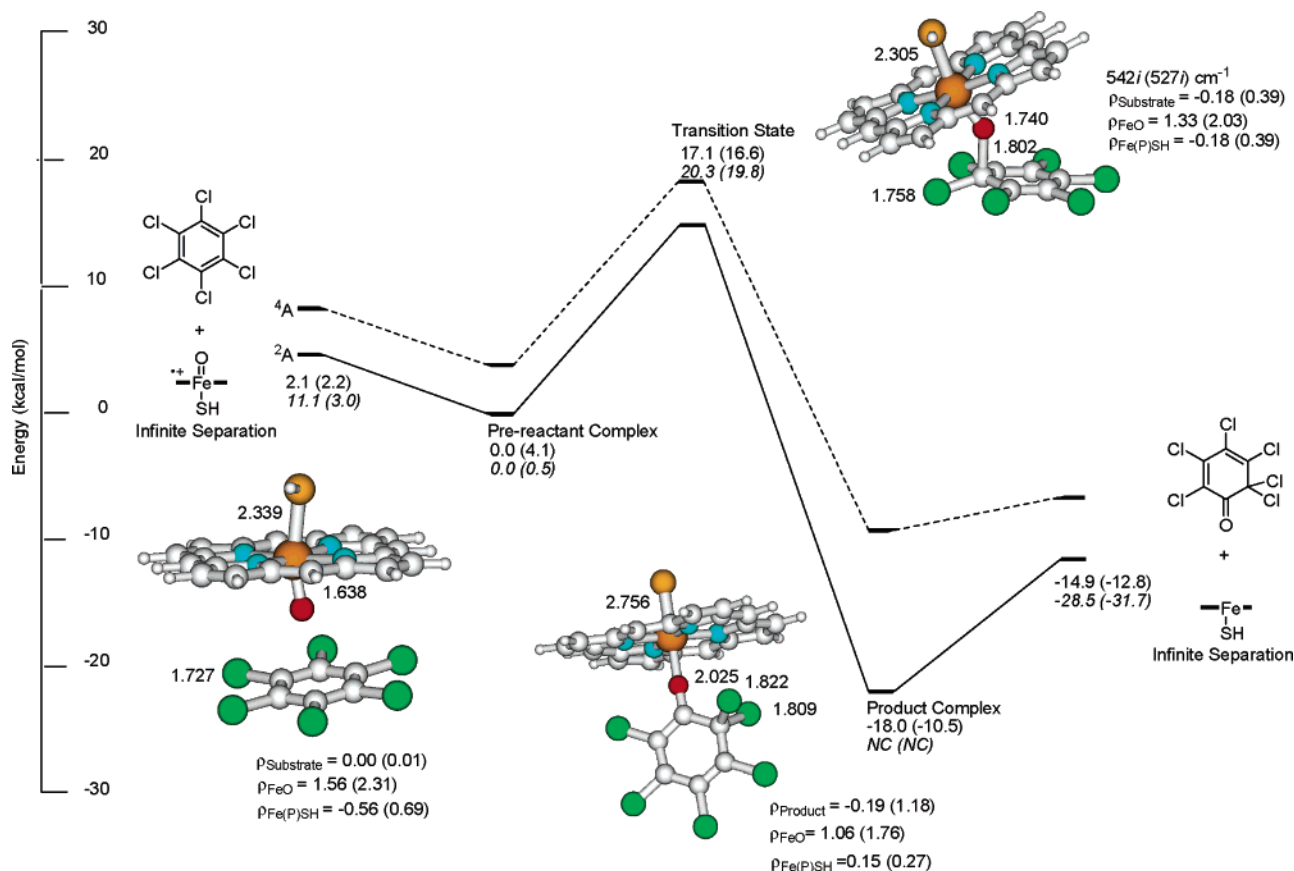


FIGURE 2: RI-PBE/TZVPP (top) and B3LYP/TZVP,SV(P) (bottom, italics) relative energy diagram of stationary points along the reaction coordinate for model Compound I addition to hexachlorobenzene. Geometries were optimized at the RI-PBE/TZVP,SV(P) level of theory. Bond distances are listed in Angstroms, and energies are in kcal/mol. The values corresponding to the quartet surface are in parentheses. NC indicates that the SCF would not converge.

to carbonyl compounds (62). The Fe–O bond distance is 1.74 Å, ~0.1 Å longer than the computed value for the pre-reactant complex, which is in close agreement to the value previously computed for the transition state for benzene oxidation (57). The ipso carbon rises 10° above the plane defined by the ortho carbon atom and chlorine atom.

These geometric parameters in the transition state for para oxidation of pentachlorophenol are similar. Compound I approaches the para carbon of pentachlorophenol at 108° with a C–O distance of 1.8 Å. The Fe–O distance is also 1.74 Å in the transition state, and the ipso carbon rises 9.8° out of the plane defined by the ortho carbons and chlorine atom. The electronic wavefunctions for the geometries of the stationary points on the RI-PBE/TZVP,SV(P) potential energy surface were recomputed in Gaussian for natural population analyses. These analyses revealed that the substrate units have moderate radical cation character in their transition states. The computed spin density localized to the C<sub>6</sub>Cl<sub>6</sub> unit in the doublet transition state is –0.18 e with a corresponding charge of +0.16 e on the aromatic unit. These values are –0.19 e and +0.25 e in the transition state on the doublet surface for pentachlorophenol oxidation. Although somewhat similar, the slightly larger spin density and charge in the case of pentachlorophenol is consistent with the expected smaller ionization potential of pentachlorophenol. Our research group has reported similar effects for hydroxyl radical addition to benzene (18) and other aromatic hydrocarbons (63).

With the exception of the intermediate connected to the transition state for ipso attack by Compound I, the primary oxidation products for the model Compound I-catalyzed reaction with hexachlorobenzene and pentachlorophenols are exothermic. The primary oxidation products, identified by distorting the transition state geometries along the normal mode associated with the single imaginary vibrational frequency with subsequent re-optimization are characterized by a concomitant 1,2-shift of the pendent chlorine atom. Triradicaloid Compound I is characterized by singly occupied, nearly degenerate  $\pi^*_{yz}$  and  $\pi^*_{xz}$ , and porphyrin “a<sub>2u</sub>” orbitals (64). “a<sub>2u</sub>” refers to the  $\pi$  orbital of the isolated porphyrin with *D*<sub>4h</sub> symmetry. Further information regarding this nomenclature for describing the electronic structure of P450 Compound I can be found in reference 64. The transformation results in a product complex characterized by a singly occupied  $\pi_{yz}$  molecular orbital localized to the FeO unit and an elongated Fe–O distance of 2.0 Å. NPA analyses reveal a small accumulation of  $\beta$  spin density and negative charge on the cyclohexadienone species within these complexes. This observation can be attributed to back-bonding from the Fe d orbitals to the  $\pi^*$  system of the cyclohexadienone ligand. Oxidation of hexachlorobenzene and pentachlorophenol at the para, meta, and ortho positions results in the formation of 2,2,3,4,5,6-hexachloro-3,5-cyclohexadienone, 4-hydroxy-2,2,3,5,6-pentachloro-3,5-cyclohexadienone, 5-hydroxy-2,2,3,4,6-pentachloro-3,5-cyclohexadienone, and 2-hydroxy-2,3,4,5,6-pentachloro-3,5-cyclohexa-

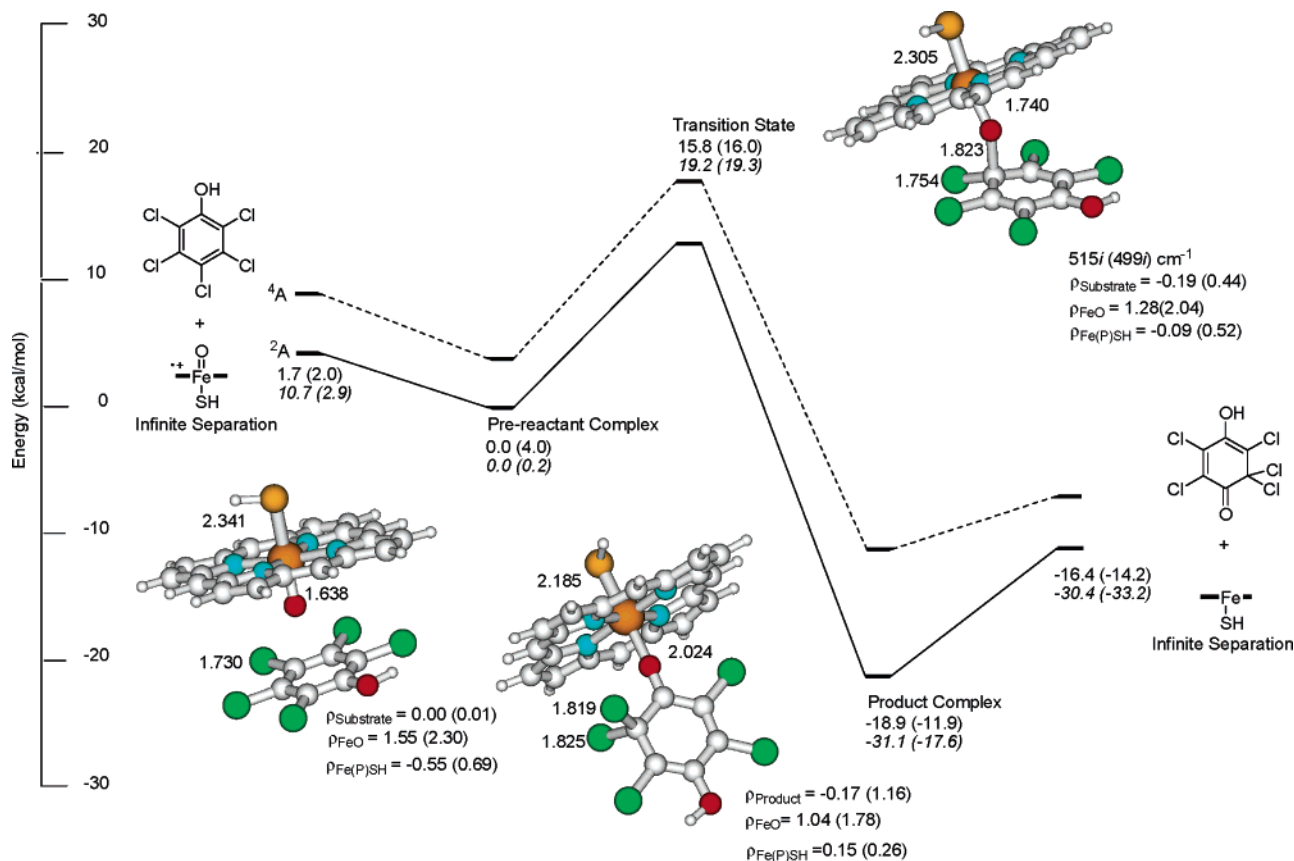
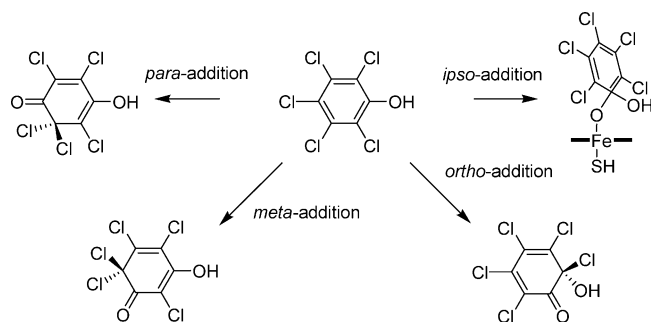


FIGURE 3: RI-PBE/TZVPP (top) and B3LYP/TZVP,SV(P) (bottom, italics) relative energy diagram of stationary points along the reaction coordinate for model Compound I addition to the para position of pentachlorophenol. Geometries were optimized at the RI-PBE/TZVP,-SV(P) level of theory. Bond distances are listed in Angstroms, and energies are in kcal/mol. The values corresponding to the quartet surface are in parentheses.

#### Scheme 3



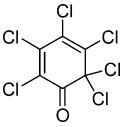
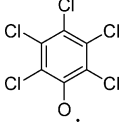
dienone, respectively. Perhalocyclohexadienone intermediates in the oxidation of perhalogenated benzenes have not previously been reported and could represent key intermediates toward the direct formation of tetrahaloquinones from P450 catalysis (Scheme 3).

The experimentally observed P450 oxidation product of hexachlorobenzene is pentachlorophenol; therefore, the formation of this product from the cyclohexadienone species requires loss of a chlorine unit. Chlorine atom or cation release has not been demonstrated for chlorinated aromatics, in contrast to the P450-catalyzed oxidation of carbon tetrachloride (65). Reduction of the cyclohexadienone species is a prerequisite for chloride ion expulsion. Reduction of this cyclohexadienone species could be enzyme- or nonenzyme-mediated. The enzyme-mediated scenario for reduction could result from electron capture from Fe(II) protoporphyrin IX previously reduced by NADPH cytochrome P450 reductase

or equivalent (66). Alternatively, the release of these species into the aqueous environment would subject them to reduction by soluble biological factors. To assess the susceptibility of 2,2,3,4,5,6-hexachloro-3,5-cyclohexadienone and the pentachlorophenoxy radical toward reduction, the vertical and adiabatic electron affinities were computed.

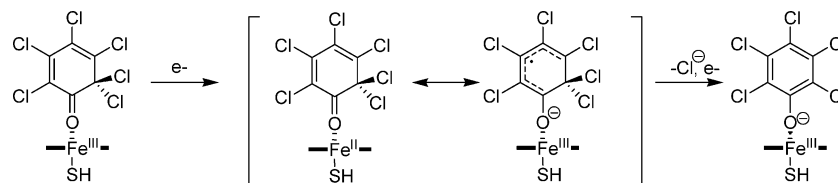
Geometries were optimized at the B3LYP/6-31G(d) level of theory and followed by single-point energy calculations with the more flexible aug-cc-pVTZ basis set. Solvation effects were included using the PCM model with  $\epsilon = 5.6$  and  $\epsilon = 78$ , with the former to mimic the hydrophobic interior of the P450 active site. These values are listed in Table 2. The electron affinity calculations of 2,2,3,4,5,6-hexachloro-3,5-cyclohexadienone indicate that this species has a significant potential for reduction with a vertical electron affinity of 2.30 eV in the gas phase. Solvation of the neutral and radical anion species result in further increases in the vertical electron affinity of 1.35 and 1.62 eV in a hydrophobic environment and water, respectively. Of particular interest is the large change in electron affinity in the hydrophobic model of the P450 interior, which supports the hypothesis that this species could effectively capture an electron from the reduced iron protoporphyrin IX. Indeed, geometry optimization of the 2,2,3,4,5,6-hexachloro-3,5-cyclohexadienone radical anion resulted in the expulsion of a chloride ion to form a complex with the pentachlorophenoxy radical. The relaxation energies range from 0.75 to 1.20 eV, indicating that electron capture by this species results in a very exothermic expulsion of the chloride ion.

Table 2: Electron Affinities<sup>a</sup> (eV) of 2,2,3,4,5,6-Hexachloro-3,5-cyclohexadienone and the Pentachlorophenoxy Radical (C<sub>2v</sub>)

				
	vertical	adiabatic	vertical	adiabatic
B3LYP/6-31G(d)	2.00	2.76	2.89	3.01
B3LYP/aug-cc-pVTZ <sup>b</sup>	2.30	3.05	3.24	3.32
PCM( $\epsilon$ = 5.6)-B3LYP/aug-cc-pVTZ <sup>b</sup>	3.65	4.69	4.67	4.75
PCM( $\epsilon$ = 78)-B3LYP/aug-cc-pVTZ <sup>b</sup>	3.92	5.12	4.97	5.05

<sup>a</sup> The vertical electron affinities are evaluated as the difference between the electronic energies of the optimized neutral geometry and the anion at the neutral geometry. The adiabatic electron affinities are evaluated as the difference in electronic energies of the optimized neutral geometry and optimized anion geometry. <sup>b</sup> B3LYP/6-31G(d) optimized geometries were used.

Scheme 4



Additionally, the resulting pentachlorophenoxy radical has a significant electron affinity, which is also augmented in the presence of both solvation models, indicating that the pentachlorophenoxy radical would be rapidly reduced to pentachlorophenoxide regardless of the enzyme's presence. Reductive dechlorination of 2,2,3,4,5,6-hexachloro-3,5-cyclohexadienone mediated by iron protoporphyrin IX is outlined in Scheme 4.

The Compound I-mediated oxidation of the pentachlorophenols would lead to a hydroxycyclohexadienone. The transformation of hydroxycyclohexadienones formed from Compound I addition do not require reduction to form the corresponding quinones. Deprotonation of the phenolic hydroxyls followed by re-optimization resulted in a facile release of chloride ion to give the tetrachloroquinones. Because one would not expect the  $pK_a$  of the hydroxycyclohexadienone to differ significantly from the pentachlorophenol value of 4.7, this deprotonation process, followed by chloride ion expulsion, would predominate at physiological pH (7.4) (67).

**Oxidation of Hexafluorobenzene and Pentafluorophenol.** The energies for the oxidation of hexafluorobenzene and pentafluorophenol are listed in Table 3. Potential energy surfaces and RI-PBE/TZVPP//RI-PBE/TZVP,SV(P) and B3LYP/TZVP,SV(P)//RI-PBE/TZVP,SV(P) energetics for Compound I addition to hexafluorobenzene and the para position of pentafluorophenol are shown in Figures 4 and 5, respectively. Potential energy surfaces for reactions at the other positions of pentafluorophenol are listed in the Supporting Information. The barrier for oxidation calculated for hexafluorobenzene at the RI-PBE level was found to be 9.2–11.8 kcal/mol on the doublet surface, and 10.2–12.4 kcal/mol on the quartet surface. Calculated barrier heights using B3LYP were 6.5 and 14.5 kcal/mol for the doublet and quartet surfaces, respectively. For both spin surfaces, the barriers were significantly lower than those obtained for the oxidation of hexachlorobenzene, a result that is consistent with the experimentally observed rates of elimination: F >

Cl > Br > I (24). In addition, an experimental study on the oxidation of chloropentafluorobenzene by microsomal cytochrome P450 demonstrated that the fluorine para to the chlorine was eliminated preferentially, and no chlorine elimination products were observed, a result that is again consistent with a lower barrier for attack at the carbon bearing the fluorine followed by loss of the fluorine (68).

Interestingly, one key difference between the oxidation of hexafluorobenzene and the above results with hexachlorobenzene was the identification of an intermediate  $\sigma$  complex (Figure 4). While hexachlorobenzene oxidation by Compound I resulted in an apparently barrierless 1,2-migration of the ipso chlorine, this migration was not observed for the oxidation of hexafluorobenzene. Instead, an intermediate cationic  $\sigma$  complex was identified, a result similar to that observed in other theoretical studies of P450-catalyzed benzene oxidation (57, 61, 69). In contrast to these results, however, the NPA charge on the aromatic substrate was found to be only  $q = 0.33$  e, whereas de Visser and Shaik found a value of  $q = 0.51$  e for the doublet surface. We attribute this result to the electron-withdrawing character of the fluorine substituents. Starting from the  $\sigma$  complex, subsequent calculations were performed to locate the transition state for fluorine migration, which was found to be 7.5 kcal/mol at the RI-PBE/TZVPP//RI-PBE/TZVP,SV(P) level of theory. From the transition state, the primary oxidation product was obtained by distorting the transition state geometry along the single imaginary vibrational mode followed by geometry optimization. The 1,2-migrated product at infinite separation was found to be more stable by 17.9 kcal/mol relative to the  $\sigma$  complex at the RI-PBE/TZVPP//RI-PBE/TZVP,SV(P) level of theory.

Potential energy surfaces were also calculated for oxidation of the four unique positions of pentafluorophenol. The potential energy surface for oxidation of the para position is shown in Figure 5. The barriers for oxidation at the ortho and para positions on the doublet surface were found to be significantly lower than that for oxidation of hexafluoroben-



Table 3: Energies (kcal/mol) Relative to the Pre-Reactant Complex on the Doublet Surface for the Oxidation of Hexafluorobenzene and Pentafluorophenol<sup>a</sup>

theory	ISR	PRC	TS	PC	ISP
hexafluorobenzene					
RI-PBE/TZVP,SV(P)	6.1 (6.9)	0.0 (4.0)	9.2 (10.2)	-9.1 (-11.5)	-20.2 (-17.9)
RI-PBE/TZVP,SV(P) + ZPE	5.6 (6.3)	0.0 (3.8)	9.3 (10.1)	-8.8 (-11.3)	-19.5 (-17.6)
RI-PBE/TZVPP	2.9 (3.2)	0.0 (4.0)	11.8 (12.4)	-6.2 (-8.3)	-24.1 (-21.9)
B3LYP/ TZVP,SV(P)	5.1 (5.1)	0.0 (-7.6)	6.5 (14.5)	-40.5 (-13.5)	-43.9 (-38.9)
<i>p</i> -pentafluorophenol					
RI-PBE/TZVP,SV(P)	5.4 (6.1)	0.0 (4.0)	7.4 (9.7)	-13.2 (-12.8)	-22.5 (-20.2)
RI-PBE/TZVP,SV(P) + ZPE	4.6 (5.7)	0.0 (3.4)	7.1 (9.9)	-13.0 (-12.4)	-22.1 (-19.7)
RI-PBE/TZVPP	2.0 (2.3)	0.0 (4.0)	9.8 (11.3)	-10.4 (-10.2)	-25.7 (-23.5)
B3LYP/ TZVP,SV(P)	4.0 (4.2)	0.0 (-7.7)	4.9 (13.2)	-21.9 (-14.6)	-46.5 (-41.6)
<i>o</i> -pentafluorophenol					
RI-PBE/TZVP,SV(P)	6.5 (7.1)	0.0 (4.2)	6.3 (8.8)	-19.1 (-15.6)	-24.9 (-22.8)
RI-PBE/TZVP,SV(P) + ZPE	6.1 (7.1)	0.0 (4.1)	6.2 (8.7)	-18.7 (-15.6)	-24.0 (-22.3)
RI-PBE/TZVPP	2.7 (3.5)	0.0 (3.4)	8.9 (11.2)	-15.2 (-11.6)	-28.3 (-25.5)
B3LYP/ TZVP,SV(P)	13.1 (5.5)	0.0 (0.0)	12.1 (13.1)	-21.0 (-16.7)	-40.0 (-42.7)
<i>m</i> -pentafluorophenol					
RI-PBE/TZVP,SV(P)	7.0 (7.4)	0.0 (4.4)	8.4 (10.2)	-10.0 (-10.1)	-23.4 (-21.5)
RI-PBE/TZVP,SV(P) + ZPE	6.6 (6.7)	0.0 (4.5)	8.6 (10.0)	-9.3 (-10.1)	-22.4 (-21.1)
RI-PBE/TZVPP	3.0 (3.2)	0.0 (4.0)	10.9 (13.4)	-6.2 (-7.3)	-27.3 (-25.1)
B3LYP/ TZVP,SV(P)	5.7 (5.3)	0.0 (-7.2)	6.8 (14.9)	-17.5 (-12.1)	-47.2 (-42.7)
<i>ipso</i> -pentafluorophenol					
RI-PBE/TZVP,SV(P)	13.6 (21.9)	0.0 (-3.6)	15.0 (26.2)	3.5 (11.7)	6.1 (16.0)
RI-PBE/TZVP,SV(P) + ZPE	14.5 (22.3)	0.0 (-3.2)	16.0 (26.7)	4.9 (12.7)	7.6 (16.5)
RI-PBE/TZVPP	8.6 (16.1)	0.0 (-3.2)	16.8 (27.2)	6.5 (13.8)	1.7 (11.1)
B3LYP/ TZVP,SV(P)	21.1 (17.2)	0.0 (-3.7)	21.1 (27.5)	5.1 (7.9)	-5.9 (-4.9)

<sup>a</sup> ISR = infinitely separated reactants, PRC = pre-reactant complex, TS = transition state, and ISP = infinitely separated products. The quartet energetics are listed in parentheses. NC = unconverged SCF.

zene, with RI-PBE-calculated heights of 6.2–8.9 and 7.1–9.8 kcal/mol, respectively. Using the B3LYP functional, these values were found to be 4.9 and 12.1 kcal/mol. Barriers calculated for the quartet surface were found to be 9.7 and 8.8 kcal/mol for ortho and para, respectively, using RI-PBE, and 13.1 and 13.2 kcal/mol, respectively, using B3LYP. The quartet surface in both cases was ~4 kcal/mol higher in energy than the doublet surface when calculated using RI-PBE. With B3LYP, the quartet surface was found to be lower in energy than the doublet surface for the pre-reactant complexes, but the higher transition state barrier indicates that the quartet surface is not likely for the reaction. As was found in the oxidation of hexafluorobenzene, the barrier heights for pentafluorophenol oxidation were generally lower by several kcal/mol when compared with those for pentachlorophenol.

On the doublet surface, meta oxidation was found to have a barrier of 8.4–10.9 kcal/mol using RI-PBE and a barrier of 6.8 kcal/mol when calculated using B3LYP. On the quartet surface, the barriers were between 10.0 and 13.4 kcal/mol when calculated using RI-PBE, and the observed barrier using B3LYP was 14.9 kcal/mol. Interestingly, although the barriers for meta attack are higher than those for ortho or para oxidation, the magnitude of the increase is significantly smaller than that observed in the chlorinated case; the difference is only 1–2 kcal/mol when calculated using RI-PBE. However, no experimental products arising from the meta oxidation of pentafluorophenol have been observed, which indicates that either this difference in barrier heights is adequate to preclude oxidation of the meta position or orientational factors in the active site are also involved in determining the regioselectivity of oxidation.

Oxidation at the ipso position of the ring was also examined and was found to have a much larger barrier on

the doublet surface of 15.0–16.8 kcal/mol using RI-PBE and 21.1 kcal/mol using B3LYP. For the quartet surface, the barrier heights were 26.2–27.2 at the RI-PBE levels of theory and 27.7 kcal/mol with B3LYP. This barrier height is not competitive with ortho or para attack. In addition, and as was the case with pentachlorophenol, the trajectory required for oxidation at this position would likely result in hydrogen-atom abstraction from the phenol as opposed to electrophilic addition to the ring.

At all four possible locations of attack, oxidation of pentafluorophenol resulted in the formation of an intermediate  $\sigma$  complex in a fashion identical to the oxidation of hexafluorobenzene. Experimental P450 studies for the oxidation of pentafluorophenol have been performed, and their results support the direct formation of tetrafluoroquinones, which rapidly react with proteins (23). To our knowledge, however, these studies have not attempted to distinguish the formation of the 1,4- and 1,2-benzoquinones from the oxidation of the para and ortho positions, respectively; in analogous studies of the oxidation of pentachlorophenol, both products are observed. Our computational results indicate that oxidation of the para and ortho positions of pentafluorophenol proceeds with the lowest barriers, a result which is consistent with both prior experimental and our current computational studies of the oxidation of pentachlorophenol. To arrive at the experimentally observed products, however, loss of fluorine is required, likely occurring after migration to an adjacent carbon.

Additional calculations were performed to examine the energetics of fluorine migration in the product of the oxidation of *para*-pentafluorophenol bound to the iron porphyrin. Given that the  $pK_a$  of the phenolic hydrogen of a perfluorinated benzene is 5.53 (67) and thus likely ionized at physiological pH, we considered both protonation states



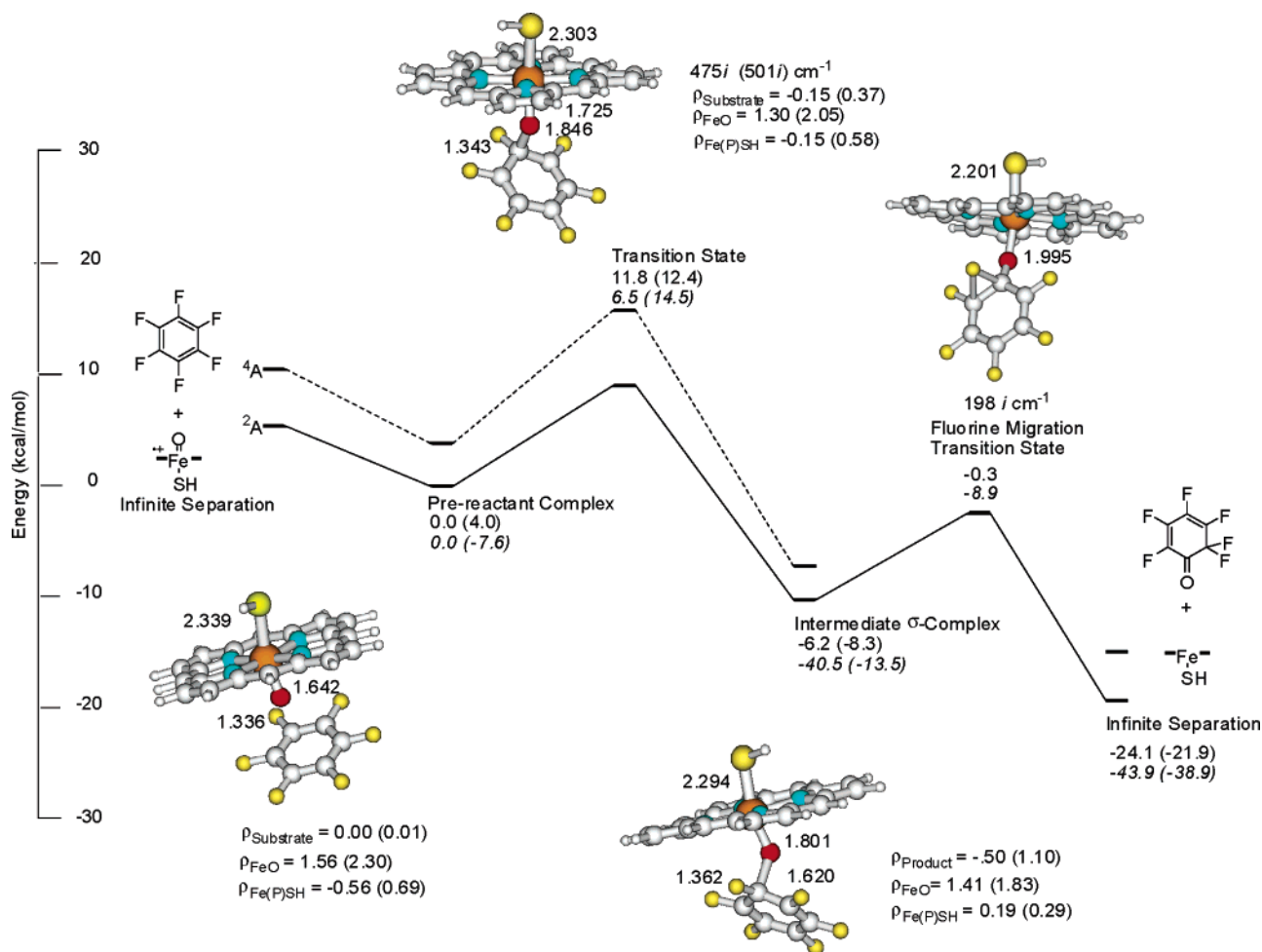


FIGURE 4: RI-PBE/TZVPP (top) and B3LYP/TZVP,SV(P) (bottom, italics) relative energy diagram of stationary points along the reaction coordinate for model Compound I addition to hexafluorobenzene. Geometries were optimized at the RI-PBE/TZVP,SV(P) level of theory. Bond distances are listed in Angstroms, and energies are in kcal/mol. The values corresponding to the quartet surface are in parentheses.

for the phenolic oxygen. The RI-PBE/TZVPP//RI-PBE/TZVP,SV(P) barrier heights for migration were found to be 18.1 kcal/mol for the deprotonated and 6.2 kcal/mol for the protonated phenol on the doublet surface. As above, the transition states were characterized by the presence of a single imaginary vibrational frequency corresponding to the reaction coordinate, and distortion along the corresponding normal mode followed by geometry optimization verified that each saddle point connected to the appropriate reactant and product on the potential energy surface. Migration was found to be energetically favorable by  $-20.1$  kcal/mol for the protonated phenol relative to the  $\sigma$  complex, whereas migration of fluorine in the deprotonated system was unfavorable by 8.7 kcal/mol. We attribute this result to the ability of the phenolate system to stabilize the cationic character of the  $\sigma$  complex via resonance (Figure 6), thereby leading to a higher activation barrier for the deprotonated phenol.

After fluorine migration, this resonance stabilization is lost, rendering migration energetically disfavored in our present model. However, in the enzyme active site, nearby residues could likely stabilize the charge on the phenolate oxygen via hydrogen bonding, making fluorine migration more energetically favorable.

NPA atomic charges were computed for all stationary points on the potential energy surfaces. As was found with hexachlorobenzene and pentachlorophenol, in the fluorinated

transition states, the aromatic substrate was found to have a moderate amount of radical character ( $\rho = -0.15$ ) for both hexafluorobenzene and pentafluorophenol. The group charges on the aromatic substrates were determined to be  $+0.19$  and  $+0.25$  e, respectively, with pentafluorophenol having a larger group charge. The same trend was observed in the chlorinated cases and as above can be attributed to the smaller ionization potential of pentafluorophenol. A comparison of the  $\sigma$  complex and cyclohexadienone product complexes indicate an accumulation of charge density on the phenolate oxygen in the migrated product, with  $q(\text{O})$  increasing from  $-0.53$  to  $-0.62$  e, a result consistent with a decrease in resonance donation upon fluorine migration. The calculated barrier of 7.4 kcal/mol for migration in the neutral pentafluorophenol is similar to the barrier calculated by Harvey and co-workers for the migration of hydrogen from the  $\sigma$  complex formed upon the oxidation of benzene (61, 69). Overall, these results indicate that fluorine migration in the P450 active site would be possible for the  $\sigma$  complex formed from Compound I addition to pentafluorophenol.

Important geometric parameters and spin densities for the reactions with hexafluorobenzene and para oxidation of pentafluorophenol are shown in Figures 4 and 5. The potential energy surfaces are products from the oxidation of pentafluorophenol qualitatively quite similar to those calculated for the oxidation of the chlorinated derivatives above,

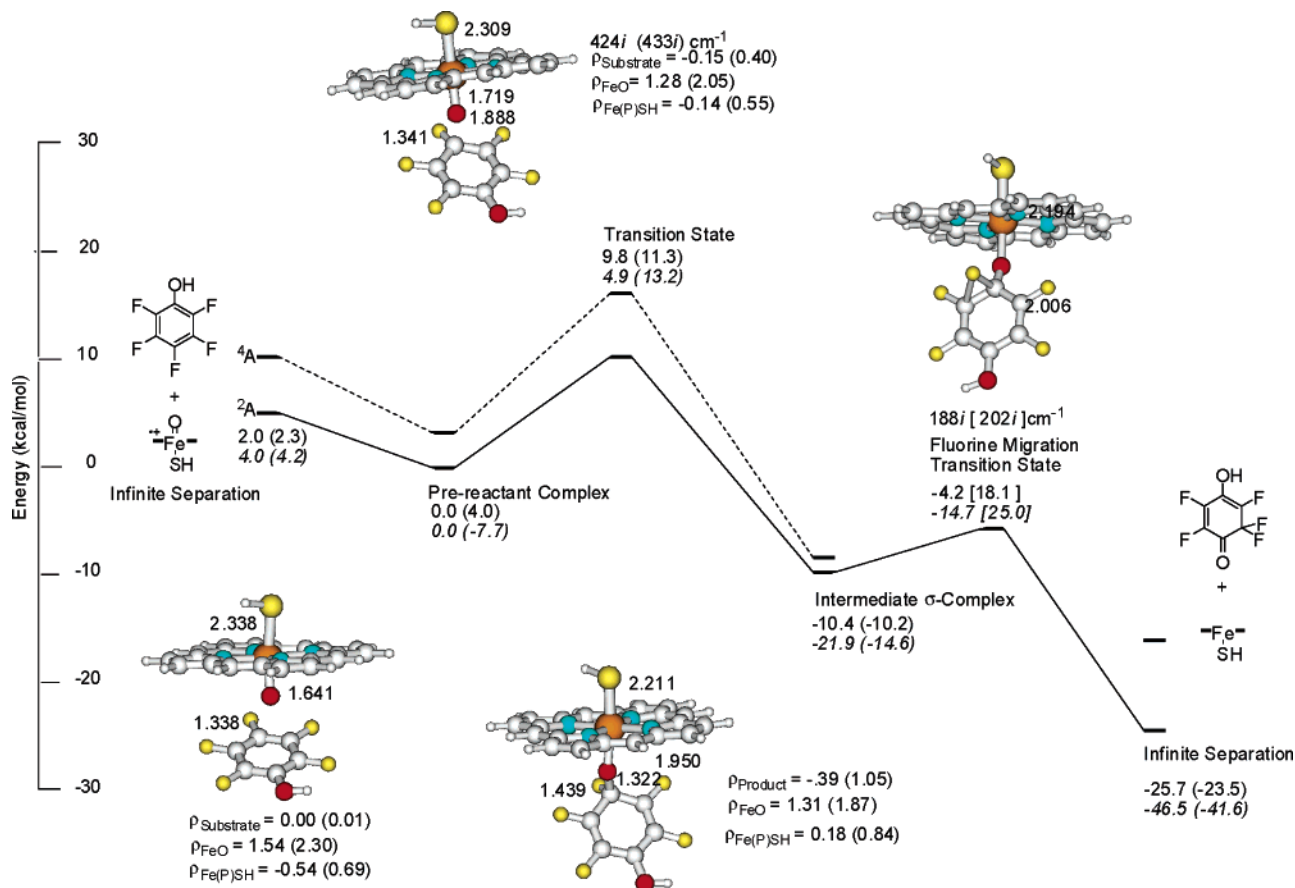


FIGURE 5: RI-PBE/TZVPP (top) and B3LYP/TZVP,SV(P) (bottom, italics) relative energy diagram of stationary points along the reaction coordinate for model Compound I addition to the para position of pentafluorophenol. Geometries were optimized at the RI-PBE/TZVP,SV(P) level of theory. Bond distances are listed in Angstroms, and energies are in kcal/mol. The values corresponding to the quartet surface are in parentheses. Transition-state barrier heights for fluorine migration in deprotonated phenol are in brackets.

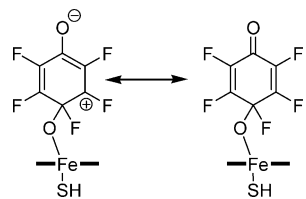


FIGURE 6: Resonance structures for the  $\sigma$  complex formed on addition to pentafluorophenolate.

with an early transition state and similar geometries. The Fe–O and O–C bond distances were found to be 1.72–1.73 and 1.85–1.89 Å, respectively, values quite similar to the 1.74 and 1.8 Å found in the chlorinated cases. In addition, the out-of-plane distortion of the ipso carbon in the transition state was found to be 9.8–10.8° out from the plane defined by its three bonded atoms, a range that matches those found with hexachlorobenzene and pentachlorophenol. The principal difference between the fluorinated results and those found for the chlorinated cases is in the angle of approach for the Compound I oxygen. In hexafluorobenzene, this angle is 102°, slightly less than the 107° in hexachlorobenzene. This trend is reproduced in the oxidation of all fluorinated positions and with all compounds.

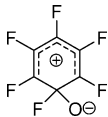
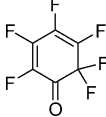
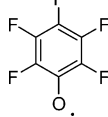
As discussed above, the principle difference in the mechanism between the chlorinated and fluorinated cases is the presence of a small barrier for 1,2-halogen migration in the fluorinated systems. Subsequent migration of fluorine was found to be thermodynamically favorable in hexafluorobenzene and all positions of neutral pentafluorophenol. The

resulting cyclohexadienones and hydroxycyclohexadienones formed upon oxidation of hexafluorobenzene and pentafluorophenol at the para, meta, and ortho positions were 2,2,3,4,5,6-hexafluoro-3,5-cyclohexadienone, 4-hydroxy-2,2,3,5,6-pentafluoro-3,5-cyclohexadienone, 5-hydroxy-2,2,3,4,6-pentafluoro-3,5-cyclohexadienone, and 2-hydroxy-2,3,4,5,6-pentafluoro-3,5-cyclohexadienone, respectively (analogous to Scheme 3, but with F instead of Cl).

Subsequent calculations were performed on the isolated products from the oxidation of hexafluorobenzene (1,2,3,4,5,6-hexafluoro-2,4-cyclohexadienone and the fluorine-migrated product, 2,2,3,4,5,6-hexafluoro-3,5-cyclohexadienone) to determine their relative energetics and other properties as well as to evaluate decomposition pathways analogous to those identified in pentachlorophenol. Furthermore, various pathways for the loss of fluorine were examined. For the isolated product molecules, the migrated product was found to be 35.9 kcal/mol lower in energy than the  $\sigma$  complex, a result that is consistent with a higher energy zwitterion converting to a neutral molecule in the gas phase.

Similar results were observed for the isolated products of the oxidation of pentafluorophenol. The initial  $\sigma$  complexes were found to be higher in energy than the product after fluorine migration. In the case of the oxidation product from *ortho*-pentafluorophenol, the migration of fluorine to the adjacent fluorine-bearing carbon was found to be favorable by 3.5 kcal/mol. Migration to the phenolic carbon was nearly thermoneutral, with an energy change of less than

Table 4: Electron Affinities<sup>a</sup> (eV) of 1,2,3,4,5,6-Hexafluoro-3,5-cyclohexadienone, 2,2,3,4,5,6-Hexafluoro-3,5-cyclohexadienone, and the Pentafluorophenoxy Radical (C<sub>2v</sub>)

						
	vertical	adiabatic	vertical	adiabatic	vertical	adiabatic
B3LYP/6-31G(d)	2.13	2.47	1.22	1.63	2.20	2.39
B3LYP/aug-cc-pVTZ <sup>b</sup>	2.86	3.21	1.92	2.28	2.90	3.05
PCM( $\epsilon$ = 5.6)-B3LYP/aug-cc-pVTZ <sup>b</sup>	4.38	4.74	3.44	3.79	4.50	4.63
PCM( $\epsilon$ = 78)-B3LYP/aug-cc-pVTZ <sup>b</sup>	4.65	5.01	3.72	4.08	4.81	4.94

<sup>a</sup> The vertical electron affinities are evaluated as the difference between the electronic energies of the optimized neutral geometry and the anion at the neutral geometry. The adiabatic electron affinities are evaluated as the difference in electronic energies of the optimized neutral geometry and optimized anion geometry. <sup>b</sup> B3LYP/6-31G(d) optimized geometries were used.

−0.01 kcal/mol. For the product of oxidation of *meta*-pentafluorophenol, migration to the para position was found to be favorable by −39.9 kcal/mol, whereas migration to the ortho position was found to be favorable by −38.1 kcal/mol. In the case of the product of the oxidation of *para*-pentafluorophenol, fluorine migration to the meta position was found to be favorable by −31.3 kcal/mol.

However, while these migrations were found to be energetically favorable, they do not directly lead to the observed final products of oxidation, namely, pentafluorophenol and tetrafluoroquinone, for the oxidation of hexafluorobenzene and pentafluorophenol, respectively. The formation of the observed products most likely requires the loss of a fluoride anion from the system, a process which requires reduction. To determine the relative reduction potentials, both vertical and adiabatic electron affinities were calculated for the isolated  $\sigma$  complex and hexafluorocyclohexadienone, using the same methods and levels of theory as previously outlined. The results of these calculations are shown in Table 4. In the case of the oxidation products of hexafluorobenzene, the  $\sigma$  complex was found to have a vertical electron affinity of 2.86 eV, with consideration of PCM solvation models ( $\epsilon$  = 5.6 and 78) increasing the value by 1.52 and 1.79 eV, respectively. Hexafluorocyclohexadienone has a somewhat smaller electron affinity of 1.92 eV in the gas phase. Analogous PCM solvation increased the electron affinities by 1.52 and 1.80 eV. The values obtained for the isolated  $\sigma$  complex were comparable with those found for hexachlorocyclohexadienone, whereas for hexafluorocyclohexadienone, the calculated electron affinities were smaller by  $\sim$ 1 eV. As was observed for the chlorinated systems above, the large electron affinities, in particular those calculated using a hydrophobic model, are indicative of the potential for trapping an electron from the reduced iron protoporphyrin IX.

A key distinction observed between the chlorinated and fluorinated cases, however, is that the loss of fluorine was *not* observed after the optimization of the reduced products. In both the isolated  $\sigma$  complex and hexafluorocyclohexadienone, optimization of the radical anions did not result in fluoride expulsion and were in fact followed by very little change in geometric parameters. Similarly, deprotonation of the phenolic oxygen in hydroxypentafluorocyclohexadienones does not lead to the loss of fluoride, which is the result observed for the hydroxypentachlorocyclohexadi-

enones. Hence, decomposition of the fluorinated analogues occurs via more complex pathways including additional barriers for fluoride loss.

Confronting these differences, we computed the thermochemistry for the loss of fluoride from the isolated  $\sigma$  complex and hydroxycyclohexadienone oxidation products of pentafluorophenol (*para*) as well as from corresponding products from hexafluorobenzene. A schematic of the considered pathways is shown in Figure 7.

Fluoride loss from hexafluorocyclohexadienone and the isolated  $\sigma$  complex in the gas phase were strongly endothermic, with calculated reaction energies of 47.5 and 28.3 kcal/mol, respectively (Figure 7a and b). Using PCM with  $\epsilon$  = 78, the energies of reaction were improved to 1.2 and −11.9 kcal/mol. Similar calculations were performed on the isolated  $\sigma$  complex and hydroxypentafluorocyclohexadienone formed from the oxidation of pentafluorophenol (Figure 7c–f). In this case, the situation is complicated by the two possible protonation states of the phenolic oxygen. Hence, we considered two possible pathways for the loss of fluoride: deprotonation of the phenolic oxygen to directly eliminate fluoride and reduction to the radical anion, which could expel fluoride leading to a neutral radical. Analogous pathways are possible for the isolated  $\sigma$  complex of pentafluorophenol; therefore, the thermochemistry of four reactions were computed. In all cases, the gas-phase energies of reaction were endothermic; however, PCM solvation again provided some stabilization of the products. The expulsion of fluoride was found to be favorable from hydroxypentafluorocyclohexadienone (Figure 7d), but this was not the case for the deprotonated hydroxypentafluorocyclohexadienone (Figure 7e).

The crystal structure of dioxygen-ligated CYP101 reveals ordered water molecules near the active site (60), which are believed to be necessary to achieve O–O bond scission (70–72). As a result, we next attempted to evaluate the energetics for the loss of fluoride from the same model systems along with two coordinating water molecules. Calculations were performed without implicit solvation models as well as using PCM with  $\epsilon$  = 78. The results of these calculations are shown in Figure 8.

With the inclusion of two waters, presolvating the reactant, and solvating the isolated fluoride, the reaction was found to be favorable by −6.6 kcal/mol and −12.5 kcal/mol for hexafluorocyclohexadienone and hydroxypentafluorocyclo-

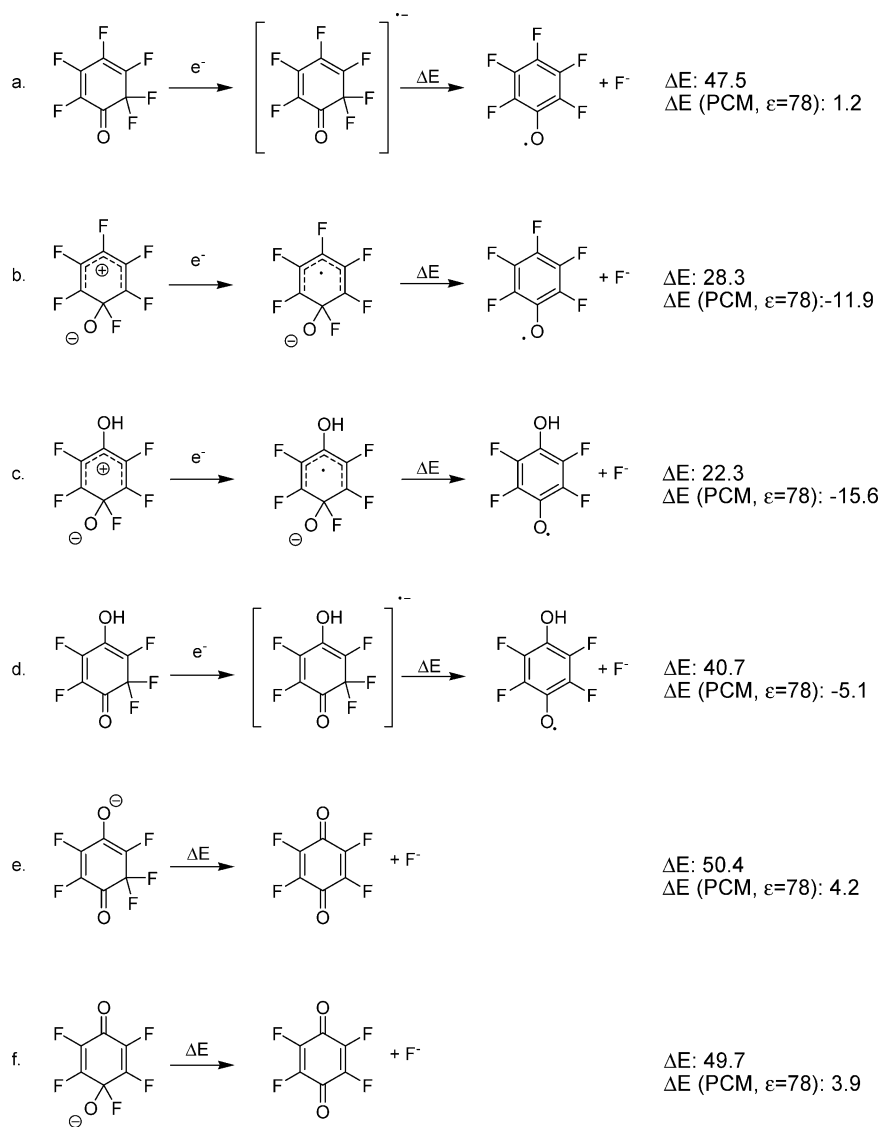


FIGURE 7: Six pathways considered for the loss of fluoride anion from the products of oxidation of hexafluorobenzene and pentafluorophenol, calculated at the B3LYP/aug-cc-pVTZ//B3LYP/6-31G\* level. Energies are given in kcal/mol.

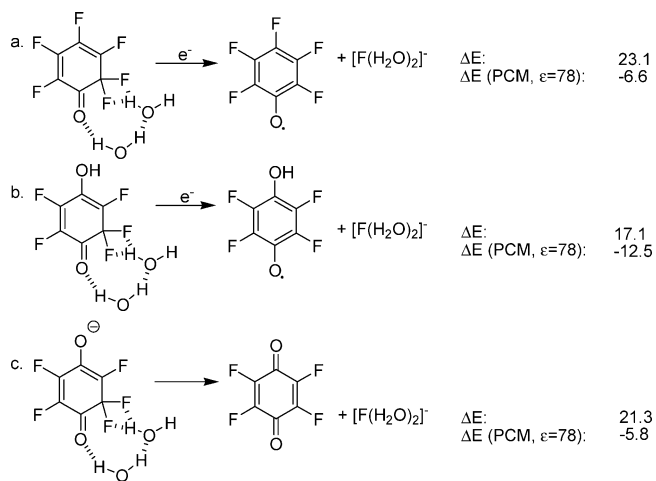


FIGURE 8: Three favorable pathways for the loss of fluoride anion from the products of oxidation of hexafluorobenzene and pentafluorophenol calculated at the B3LYP/aug-cc-pVTZ//B3LYP/6-31G\* level of theory. Energies are given in kcal/mol.

hexadienone radical anions, respectively, using PCM in conjunction with explicit water molecules (Figure 8a and b). For the deprotonated phenolate, the reaction was favorable

by  $-5.8$  kcal/mol with PCM (Figure 8c). It should be noted that in the active site cavity, the phenolic oxygen could likely be stabilized by hydrogen-bond donors, which would likely result in the reaction energetics becoming more favorable as its electronic structure becomes more akin to that of hydroxypentafluorocyclohexadienone. In both cases, however, the loss of fluoride was found to be energetically favorable. After the loss of fluoride in the sequence shown in Figure 8a, the formation of the experimentally observed product, pentafluorophenol, requires only hydrogen-atom abstraction by the oxygen-centered radical, a process that would likely be quite rapid. Alternatively, the pentafluorophenoxyl radical has a significant electron affinity (Table 5), which could be reduced to pentafluorophenolate. The situation is somewhat more complex for the products formed in the sequences shown in Figure 8b and c. The experimentally observed product of the oxidation of pentafluorophenol by cytochrome P450 is tetrafluorohydroquinone. However, it has been suggested that the formation of this product is preceded by the generation of a reactive intermediate, most likely tetrafluoroquinone (23). If the reaction sequence in Figure 8b dominates, then the oxygen



Table 5: Energies (kcal/mol) Relative to the Pre-Reactant Complex on the Doublet Surface for the Oxidation of Chlorofluorobenzenes<sup>a</sup>

theory	ISR	PRC	TS	PC	ISP
chloropentafluorobenzene Cl oxidation					
RI-PBE/TZVP,SV(P)	5.7 (6.5)	0.0 (4.0)	12.5 (16.2)	-25.5 (-18.2)	-14.0 (-11.6)
RI-PBE/TZVP,SV(P) + ZPE	5.4 (6.1)	0.0 (3.7)	12.1 (15.8)	-24.2 (-17.9)	-13.6 (-11.6)
RI-PBE/TZVPP	2.4 (3.0)	0.0 (3.6)	14.5 (17.9)	-21.7 (-15.7)	-17.6 (-15.0)
B3LYP/ TZVP,SV(P)	4.3 (5.0)	0.0 (-8.3)	11.0 (36.7)	-38.4 (-17.4)	-37.4 (-31.7)
chloropentafluorobenzene <i>p</i> -F oxidation					
RI-PBE/TZVP,SV(P)	5.9 (6.6)	0.0 (4.1)	7.4 (9.6)	-10.8 (-12.1)	-13.8 (-11.5)
RI-PBE/TZVP,SV(P) + ZPE	5.6 (6.3)	0.0 (3.7)	7.3 (9.5)	-10.6 (-11.8)	-13.4 (-11.4)
RI-PBE/TZVPP	2.5 (2.8)	0.0 (4.0)	10.1 (11.7)	-17.0 (-9.0)	-17.4 (-15.2)
B3LYP/ TZVP,SV(P)	4.2 (4.7)	0.0 (-8.1)	6.3 (NC)	-10.1 (-14.0)	-37.4 (-32.0)
1,3,5-trichloro-2,4,6-trifluorobenzene Cl oxidation					
RI-PBE/TZVP,SV(P)	5.7 (6.2)	0.0 (4.3)	15.0 (16.2)	-24.7 (-18.3)	-13.3 (-11.2)
RI-PBE/TZVP,SV(P) + ZPE	5.3 (5.9)	0.0 (3.9)	14.2 (15.5)	-24.2 (-18.4)	-13.3 (-11.5)
RI-PBE/TZVPP	2.4 (2.5)	0.0 (4.1)	25.1 (17.3)	-21.5 (-15.7)	-16.8 (-14.8)
B3LYP/ TZVP,SV(P)	12.4 (4.1)	0.0 (0.6)	20.4 (21.3)	-29.6 (-10.6)	-28.4 (-31.8)
1,3,5-trichloro-2,4,6-trifluorobenzene F oxidation					
RI-PBE/TZVP,SV(P)	5.8 (5.8)	0.0 (4.7)	10.5 (10.3)	-7.1 (-10.0)	-13.6 (-12.0)
RI-PBE/TZVP,SV(P) + ZPE	5.4 (5.5)	0.0 (4.3)	9.9 (9.8)	-7.5 (-9.8)	-13.7 (-12.3)
RI-PBE/TZVPP	2.5 (2.6)	0.0 (4.1)	12.2 (12.2)	-4.3 (-6.6)	-17.4 (-15.4)
B3LYP/ TZVP,SV(P)	4.3 (4.4)	0.0 (-7.7)	7.8 (28.5)	-16.8 (-10.4)	-37.3 (-32.2)

<sup>a</sup> ISR = infinitely separated reactants, PRC = pre-reactant complex, TS = transition state, and ISP = infinitely separated products. The quartet energetics are listed in parentheses. NC = unconverged SCF.

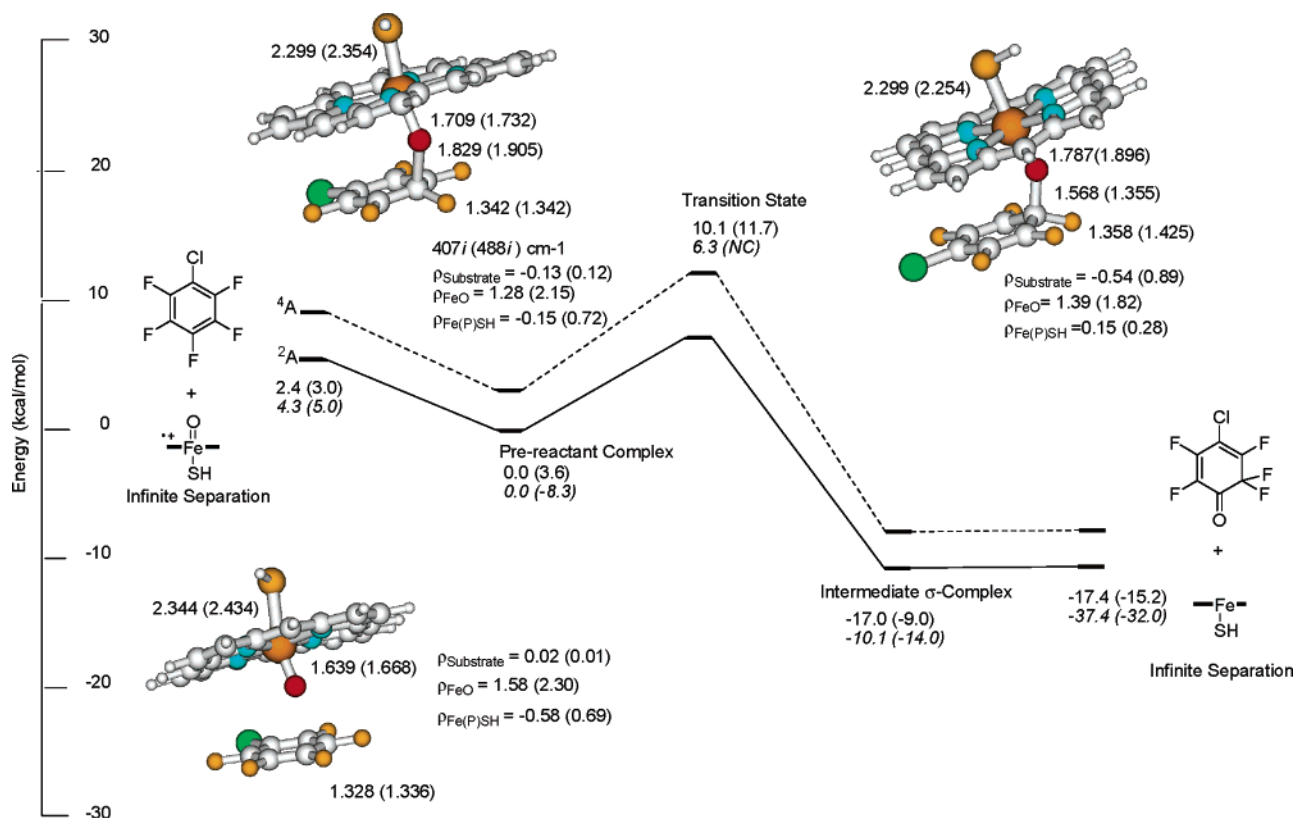


FIGURE 9: RI-PBE/TZVPP (top) and B3LYP/TZVP,SV(P) (bottom, italics) relative energy diagram of stationary points along the reaction coordinate for model Compound I addition to the para position of chloropentafluorobenzene. Geometries were optimized at the RI-PBE/TZVP,SV(P) level of theory. Bond distances are listed in Angstroms, and energies are in kcal/mol. The values corresponding to the quartet surface are in parentheses.

will likely abstract a hydrogen atom to form tetrafluorosemiquinone, which is a likely precursor to tetrafluorohydroquinone, rather than the tetrafluorobenzoquinone. If, instead, the pathway in Figure 8c dominates, then tetrafluorobenzoquinone is directly formed. There are still a few uncertainties, however. The calculations were performed on the isolated product, no longer associated with the P450 enzyme. It is

possible that fluorine could be lost while the cyclohexadienone was still in the P450 active site.

**Oxidation of Chlorofluorobenzenes.** *In vitro* and *in vivo* rat biotransformation studies of chloropentafluorobenzene and 1,3,5-trifluoro-2,4,6-trichlorobenzene by cytochrome P450 have been performed and the products characterized by <sup>19</sup>F NMR spectroscopy (68). *para*-Chlorotetrafluorophenol

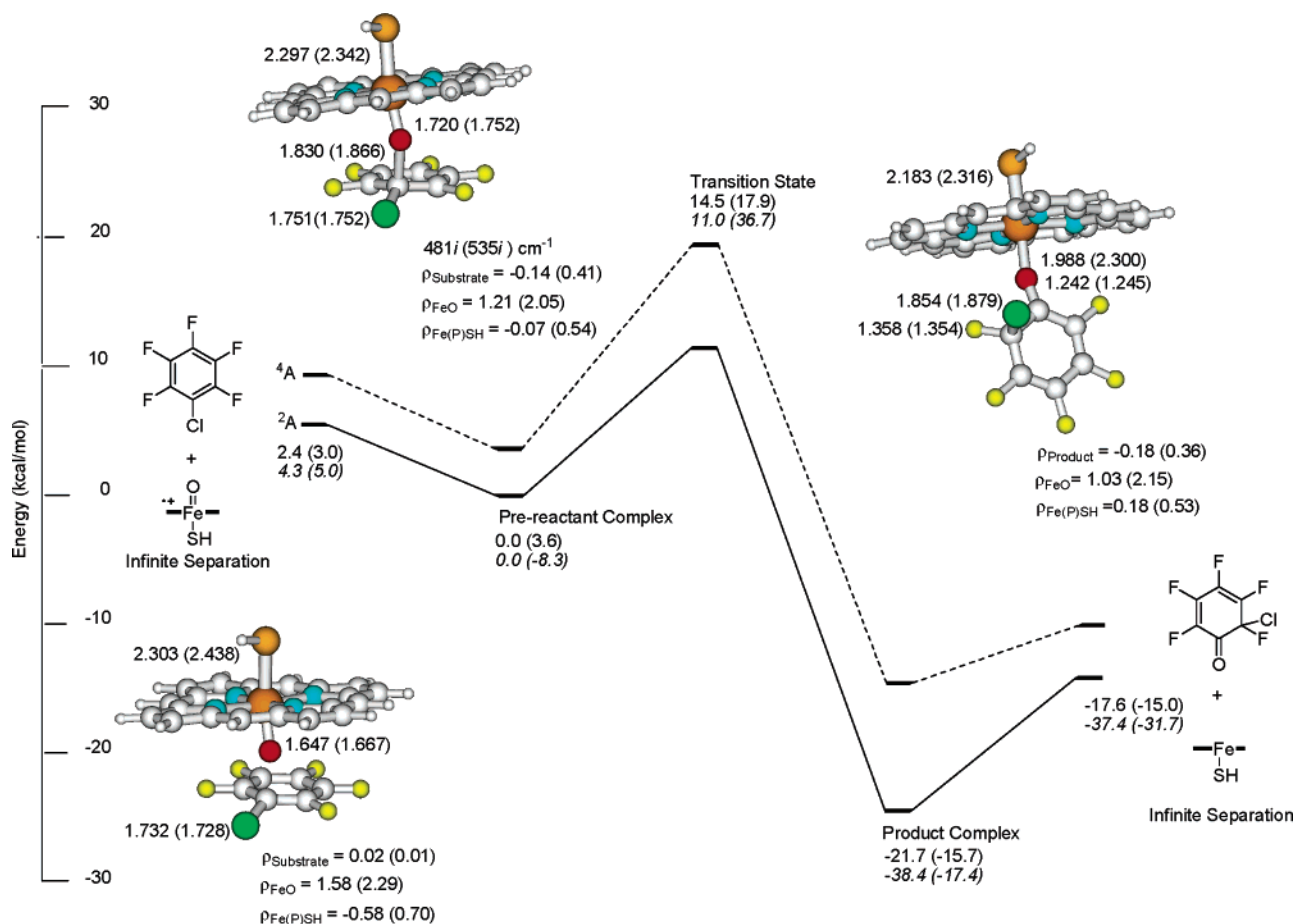


FIGURE 10: RI-PBE/TZVPP (top) and B3LYP/TZVP,SV(P) (bottom, italics) relative energy diagram of stationary points along the reaction coordinate for model Compound I addition to the chlorinated position of chloropentafluorobenzene. Geometries were optimized at the RI-PBE/TZVP,SV(P) level of theory. Bond distances are listed in Angstroms, and energies are in kcal/mol. The values corresponding to the quartet surface are in parentheses.

and its phase II reaction products were identified as the primary metabolites in rat urine, demonstrating the preferential elimination of the *p*-F atom in the metabolism of chloropentafluorobenzene. In similar *in vivo* 1,3,5-trifluoro-2,4,6-trichlorobenzene biotransformation experiments, only 1,3-difluoro-2,4,6-trichlorophenol and its corresponding phase II metabolites were observed. *In vitro* studies of chloropentafluorobenzene biotransformation by rat liver microsomal P450 also demonstrated preferential elimination of the *p*-F atom to give *para*-chlorotetrafluorophenol. Previous theoretical work on the oxidation of benzene and monosubstituted analogues (57, 61, 69) as well as the results presented here for hexachlorobenzene and hexafluorobenzene indicate that the rate-determining step in P450 oxidation of benzenes is the addition of Compound I to the aromatic ring; thus, we computed the potential energy surfaces for the oxidation of these mixed F/Cl compounds whose oxidative metabolism has been experimentally considered.

For chloropentafluorobenzene, we considered the addition of Compound I to the *p*-F substituted position as well as the chlorinated position, and the potential energy surfaces for these processes are shown in Figures 9 and 10. For the following discussion, we will only mention the RI-PBE activation barriers; the corresponding B3LYP barriers are in Table 4. The barriers for this process were consistently lower for addition to the *p*-F position for all levels of theory examined. Barriers for addition to the *p*-F position were 7.4–

10.1 kcal/mol on the doublet surface and 9.5–11.7 on the quartet surface. Barriers for addition to the chlorinated position were computed to be 12.1–14.5 kcal/mol on the doublet surface and 15.8–17.9 kcal/mol on the quartet surface. We also computed the potential energy surface for the addition of Compound I to both fluorinated and chlorinated positions on 1,3,5-trifluoro-2,4,6-trichlorobenzene. Oxidation of a fluorinated position in this case was again energetically preferred, with barriers for addition to the fluorinated position of 9.9–12.2 kcal/mol on the doublet surface and 9.8–12.2 kcal/mol on the quartet surface, as compared to addition to a chlorinated position for which the barriers were computed to be 14.2–25.1 kcal/mol on the doublet surface and 15.5–17.3 kcal/mol on the quartet surface. As in the previously described perhalogenated benzenes and phenol, oxidation at a chlorine-bearing carbon resulted in an apparently barrierless shift of the chlorine to the adjacent atom, and transition states for oxidation at a fluorine-bearing carbon could be connected to intermediate  $\sigma$  complexes. Despite the small number of compounds considered to validate the ability of these theoretical methods to predict the regiospecificity of P450 metabolism, these results are encouraging and consistent with experiments.

## CONCLUSIONS

We have presented a density functional theory study of the mechanisms by which cytochrome P450 Compound I

oxidizes perchlorinated and perfluorinated benzenes to phenols and subsequently to benzoquinones. The computationally efficient resolution-of-the-identity method with the PBE density functional is predictive of the triradicaloid electronic structure of P450 Compound I, similar to the B3LYP density functional, which does not benefit from this approximation. A novel mechanism has been identified by which perhalogenated benzenes are transformed directly into tetrahaloquinones. The addition of P450 Compound I to chlorinated positions of the hexahalogenated species considered in this study resulted in an apparently barrierless migration to the adjacent carbon yielding a perhalocyclohexadienone coordinated to the Fe via the carbonyl group. The relative barriers for the addition to nonequivalent positions of pentachlorophenol were consistent with the observation of only ortho and para oxidation products experimentally. Conclusions drawn from these calculations do not consider the contributions of the P450 reduction rate, substrate binding and orientation, formation of oxygen intermediates, rates of product release, and other processes to the observed product distribution. However, we hypothesize that the addition of the Compound I oxygen to the aromatic ring is at least partially rate-determining because of the correlation of our results with available experimental data. Computation of the electron affinities of hexachlorocyclohexadienone and the pentachlorophenoxy radical revealed that these species could be reduced efficiently by enzymatic or nonenzymatic mediated mechanisms. The hexachlorocyclohexadienone radical anion undergoes facile expulsion of chloride to form the pentachlorophenoxy radical, an obvious precursor to the experimentally observed pentachlorophenolate product. Moreover, the products of pentachlorophenol oxidation, the hydroxypentachlorocyclohexadienones, expel chloride to directly form the tetrachloroquinones upon deprotonation of the hydroxyl functionality.

Compound I addition to hexafluorobenzene and pentafluorophenol results in the formation of a characteristic  $\sigma$  complex intermediate like that previously computed for hydrogen-bearing positions of benzene and monosubstituted analogues (61). Interestingly, the barrier computed for the formation of this intermediate is smaller than that previously computed, and also verified by us, for hydrogen-bearing positions. The pendent fluorine atom of the  $\sigma$  complex migrates with a moderate barrier to form hexafluorocyclohexadienones and hydroxypentafluorocyclohexadienones from hexafluorobenzene and pentafluorophenol, respectively. Unlike the analogous perchlorinated species, the radical anion of hexafluorocyclohexadienone does not spontaneously lose fluoride in the gas phase. Additionally, deprotonation of the hydroxypentafluorocyclohexadienones does not decompose to fluoride and tetrafluoroquinone in a facile manner. Thermochemical calculations support the conclusion that explicit coordination by water molecules is necessary in order for fluoride expulsion to be energetically favorable.

These theoretical approaches predicted the experimentally observed preferential oxidation of the para-fluorinated position of chloropentafluorobenzene and of one of the three equivalent fluorinated positions of 1,3,5-trichloro-2,4,6-trifluorobenzene. Despite the small number of molecules considered in this study, the results presented here underscore the importance that these theoretical methods could play in the prediction of the chemoselectivity of xenobiotic metabo-

lism by cytochrome P450 enzymes combined with the ever-increasing knowledge of mammalian P450 enzyme structure (73). This study also demonstrates that cytochrome P450 Compound I is an effective oxidant toward these perhalogenated aromatic species as it is toward hydrocarbons. This knowledge illustrates the importance of ongoing P450 protein-engineering efforts to develop enzymes with improved kinetics toward these substrates, and such enzymes could have broad applications including environmental remediation and chemical synthesis.

## ACKNOWLEDGMENT

The authors are indebted to the Ohio Supercomputer Center for computational resources.

## SUPPORTING INFORMATION AVAILABLE

Additional computational data and Cartesian coordinates of the geometries discussed herein. This material is free of charge via the Internet at <http://pubs.acs.org>.

## REFERENCES

- Kimbrough, R. D. (1995) Polychlorinated biphenyls (PCBs) and human health: an update, *Crit. Rev. Toxicol.* 25, 133–163.
- Evangelista de Duffard, A. M., and Duffard, R. (1996) Behavioral toxicology, risk assessment, and chlorinated hydrocarbons, *Environ. Health Perspect.* 104, 353–360.
- Janssen, D. B., Oppentocht, J. E., and Poelarends, G. J. (2001) Microbial dehalogenation, *Curr. Opin. Biotechnol.* 12, 254–258.
- Lee, M. D., Odom, J. M., and Buchanan, R. J., Jr. (1998) New perspectives on microbial dehalogenation of chlorinated solvents: insights from the field, *Annu. Rev. Microbiol.* 52, 423–452.
- Fetznier, S. (1998) Bacterial dehalogenation, *Appl. Microbiol. Biotechnol.* 50, 633–657.
- Commandeur, L. C., and Parsons, J. R. (1990) Degradation of halogenated aromatic compounds, *Biodegradation* 1, 207–220.
- Motosugi, K., and Soda, K. (1983) Microbial degradation of synthetic organochlorine compounds, *Experientia* 39, 1214–1220.
- Smidt, H., and de Vos, W. M. (2004) Anaerobic microbial dehalogenation, *Annu. Rev. Microbiol.* 58, 43–73.
- Bell, S. G., Chen, X., Xu, F., Rao, Z., and Wong, L. L. (2003) Engineering substrate recognition in catalysis by cytochrome P450cam, *Biochem. Soc. Trans.* 31, 558–562.
- Stevenson, J.-A., Westlake, A. C. G., Whittock, C., and Wong, L.-L. (1996) The catalytic oxidation of linear and branched alkanes by cytochrome P450cam, *J. Am. Chem. Soc.* 118, 12846–12847.
- Nickerson, D. P., Harford-Cross, C. F., Fulcher, S. F., and Wong, L.-L. (1997) The catalytic activity of cytochrome P450cam towards styrene oxidation is increased by site-specific mutagenesis, *FEBS Lett.* 405, 153–156.
- England, P. A., Harford-Cross, C. F., Stevenson, J.-A., Rouch, D. A., and Wong, L.-L. (1998) The oxidation of naphthalene and pyrene by cytochrome P450cam, *FEBS Lett.* 424, 271–274.
- Harford-Cross, C. F., Carmichael, A. B., Allan, F. K., England, P. A., Rouch, D. A., and Wong, L.-L. (2000) Protein engineering of cytochrome p450cam (CYP101) for the oxidation of polycyclic aromatic hydrocarbons, *Protein Eng.* 13, 121–128.
- Jones, J. P., O'Hare, E. J., and Wong, L.-L. (2001) Oxidation of polychlorinated benzenes by genetically engineered CYP101 (cytochrome P450(cam)), *Eur. J. Biochem.* 268, 1460–1467.
- Walsh, M. E., Kyritsis, P., Eady, N. A. J., Hill, A. O., and Wong, L.-L. (2000) Catalytic reductive dehalogenation of hexachloroethane by molecular variants of cytochrome P450cam (CYP101), *Eur. J. Biochem.* 267, 5815–5820.
- Chen, X., Christopher, A., Jones, J. P., Bell, S. G., Guo, Q., Xu, F., Rao, Z., and Wong, L.-L. (2002) Crystal structure of the F87W/Y96F/V247L mutant of cytochrome P-450cam with 1,3,5-trichlorobenzene bound and further protein engineering for the oxidation of pentachlorobenzene and hexachlorobenzene, *J. Biol. Chem.* 277, 37519–37526.



17. Rietjens, I. M. C. M., den Besten, C., Hanzlik, R. P., and van Bladeren, P. J. (1997) Cytochrome P450-catalyzed oxidation of halobenzene derivatives, *Chem. Res. Toxicol.* **10**, 629–635.
18. DeMatteo, M. P., Poole, J. S., Shi, X., Sachdeva, R., Hatcher, P. G., Hadad, C. M., and Platz, M. S. (2005) On the electrophilicity of hydroxyl radical: a laser flash photolysis and computational study, *J. Am. Chem. Soc.* **127**, 7094–7109.
19. Van Ommen, B., Adang, A. E. P., Brader, L., Posthumus, M. A., Müller, F., and Van Bladeren, P. J. (1986) The microsomal metabolism of hexachlorobenzene. Origin of the covalent binding to protein, *Biochem. Pharmacol.* **35**, 3233–3238.
20. Van Ommen, B., Adang, A., Muller, F., and van Bladeren, P. J. (1986) The microsomal metabolism of pentachlorophenol and its covalent binding to protein and DNA, *Chem.-Biol. Interact.* **60**, 1–11.
21. Van Ommen, B., and Van Bladeren, P. J. (1989) Possible reactive intermediates in the oxidative biotransformation of hexachlorobenzene, *Drug Metab. Drug Interact.* **7**, 213–243.
22. Cnubben, N. H. P., Vervoort, J., Boersma, M. G., and Rietjens, I. M. C. M. (1995) The effect of varying halogen substituent patterns on the cytochrome P450 catalyzed dehalogenation of 4-halogenated anilines to 4-aminophenol metabolites, *Biochem. Pharmacol.* **49**, 1235–1248.
23. den Besten, C., van Bladeren, P. J., Duizer, E., Vervoort, J., and Rietjens, I. M. C. M. (1993) Cytochrome P450-mediated oxidation of pentafluorophenol to tetrafluorobenzquinone as the primary reaction product, *Chem. Res. Toxicol.* **6**, 674–680.
24. Ohe, T., Mashino, T., and Hirobe, M. (1995) Application of chemical P450 model systems to study on drug metabolism. IV. Novel oxidative pathway of para-substituted ipso-substitution by the oxygen atom of the active species, *Tetrahedron Lett.* **36**, 7681–7684.
25. Schöneboom, J. C., Lin, H., Reuter, N., Thiel, W., Cohen, S., Ogliaro, F., and Shaik, S. (2002) The elusive oxidant species of cytochrome P450 enzymes: characterization by combined quantum mechanical/molecular mechanical (QM/MM) calculations, *J. Am. Chem. Soc.* **124**, 8142–8151.
26. Hackett, J. C., Brueggemeier, R. W., and Hadad, C. M. (2005) The final catalytic step of cytochrome P450 aromatase: a density functional theory study, *J. Am. Chem. Soc.* **127**, 5224–5237.
27. Ahlrichs, R., Bär, M., Häser, M., Horn, H., and Kölmel, C. (1989) Electronic structure calculations on workstation computers: the program system TURBOMOLE, *Chem. Phys. Lett.* **62**, 165–169; for the current version of TURBOMOLE, see <http://www.turbomole.de>.
28. Häser, M., and Ahlrichs, R. (1989) Improvements on the direct SCF method, *J. Comput. Chem.* **10**, 104–111.
29. Treutler, O., and Ahlrichs, R. (1995) Efficient molecular numerical integration schemes, *J. Chem. Phys.* **102**, 346–354.
30. Arnim, M. v., and Ahlrichs, R. (1998) Performance of parallel TURBOMOLE for density functional calculations, *J. Comput. Chem.* **19**, 1746–1757.
31. Perdew, J. P., and Wang, Y. (1992) Accurate and simple analytic representation of the electron-gas correlation energy, *Phys. Rev. B: Condens. Matter* **45**, 13244–13249.
32. Perdew, J. P., Burke, K., and Ernzerhof, M. (1996) Generalized gradient approximation made simple, *Phys. Rev. Lett.* **77**, 3865–3868.
33. Eichkorn, K., Treutler, O., Öhm, H., Häser, M., and Ahlrichs, R. (1995) Auxiliary basis sets to approximate Coulomb potentials, *Chem. Phys. Lett.* **242**, 652–660.
34. Eichkorn, K., Weigend, F., Treutler, O., and Ahlrichs, R. (1997) Auxiliary basis sets for main row atoms and transition metals and their use to approximate Coulomb potentials, *Theor. Chem. Acc.* **97**, 119–124.
35. Ahlrichs, R. (2004) Efficient evaluation of three-center two-electron integrals over Gaussian functions, *Phys. Chem. Chem. Phys.* **6**, 5119–5121.
36. Swart, M., Groenhof, A. R., Ehlers, A. W., and Lammertsma, K. (2004) Validation of exchange-correlation functionals for spin states of iron complexes, *J. Phys. Chem. A* **108**, 5479–5483.
37. Schäfer, A., Horn, H., and Ahlrichs, R. (1992) Fully optimized contracted Gaussian basis sets for atoms Li to Kr, *J. Chem. Phys.* **97**, 2571–2577.
38. Schäfer, A., Huber, C., and Ahlrichs, R. (1994) Fully optimized contracted Gaussian basis sets of triple zeta valence quality for atoms Li to Kr, *J. Chem. Phys.* **100**, 5829–5835.
39. Stevens, P. J., Devlin, F. J., Chablowski, C. F., and Frisch, M. J. (1994) Ab initio calculation of vibrational absorption and circular dichroism spectra using density functional force fields, *J. Phys. Chem.* **98**, 11623–11627.
40. Becke, A. D. (1993) Density-functional thermochemistry. III. The role of exact exchange, *J. Chem. Phys.* **98**, 5648–5652.
41. Becke, A. D. (1992) Density-functional thermochemistry. I. The effect of the exchange-only gradient correction, *J. Chem. Phys.* **96**, 2155–2160.
42. Becke, A. D. (1992) Density-functional thermochemistry. II. The effect of the Perdew–Wang generalized-gradient correlation correction, *J. Chem. Phys.* **97**, 9173–9177.
43. Lee, C., Yang, W., and Parr, R. G. (1988) Development of the Colle-Salvetti correlation-energy formula into a functional of the electron density, *Phys. Rev. B: Condens. Matter* **37**, 785–789.
44. Frisch, M. J., Trucks, G. W., Schlegel, H. B., Scuseria, G. E., Robb, M. A., Cheeseman, J. R., Montgomery, J. A., Jr., Vreven, T., Kudin, K. N., Burant, J. C., Millam, J. M., Iyengar, S. S., Tomasi, J., Barone, V., Mennucci, B., Cossi, M., Scalmani, G., Rega, N., Petersson, G. A., Nakatsuji, H., Hada, M., Ehara, M., Toyota, K., Fukuda, R., Hasegawa, J., Ishida, M., Nakajima, T., Honda, Y., Kitao, O., Nakai, H., Klene, M., Li, X., Knox, J. E., Hratchian, H. P., Cross, J. B., Bakken, V., Adamo, C., Jaramillo, J., Gomperts, R., Stratmann, R. E., Yazyev, O., Austin, A. J., Cammi, R., Pomelli, C., Ochterski, J. W., Ayala, P. Y., Morokuma, K., Voth, G. A., Salvador, P., Dannenberg, J. J., Zakrzewski, V. G., Dapprich, S., Daniels, A. D., Strain, M. C., Farkas, O., Malick, D. K., Rabuck, A. D., Raghavachari, K., Foresman, J. B., Ortiz, J. V., Cui, Q., Baboul, A. G., Clifford, S., Cioslowski, J., Stefanov, B. B., Liu, G., Liashenko, A., Piskorz, P., Komaromi, I., Martin, R. L., Fox, D. J., Keith, T., Al-Laham, M. A., Peng, C. Y., Nanayakkara, A., Challacombe, M., Gill, P. M. W., Johnson, B., Chen, W., Wong, M. W., Gonzalez, C., Pople, J. A. (2004) *Gaussian 03*, revision C.02, Gaussian, Inc., Wallingford, CT.
45. Miertus, S., Scrocco, E., and Tomasi, J. (1981) Electrostatic interaction of a solute with a continuum. A direct utilization of ab initio molecular potentials for the prevision of solvent effects, *J. Chem. Phys.* **55**, 117–129.
46. Miertus, S., and Tomasi, J. (1982) Approximate evaluations of the electrostatic free energy and internal energy changes in solution processes, *Chem. Phys.* **65**, 239–245.
47. Cossi, M., Barone, V., Cammi, R., and Tomasi, J. (1996) Ab initio study of solvated molecules: a new implementation of the polarizable continuum model, *Chem. Phys. Lett.* **255**, 327–335.
48. Tomasi, J., Mennucci, B., and Cammi, R. (2005) Quantum mechanical continuum solvation models, *Chem. Rev.* **105**, 2999–3094.
49. Tomasi, J., and Persico, M. (1994) Molecular interactions in solution: An overview of methods based on continuous distributions of the solvent, *Chem. Rev.* **94**, 2027–2094.
50. Deglmann, P., Furche, F., and Ahlrichs, R. (2002) An efficient implementation of second analytical derivatives for density functional methods, *Chem. Phys. Lett.* **362**, 511–518.
51. Reed, A. E., Weinstock, R. B., and Weinhold, F. (1985) Natural population analysis, *J. Chem. Phys.* **83**, 735–746.
52. Neese, F. (2003) A spectroscopy oriented configuration interaction procedure, *J. Chem. Phys.* **119**, 9428–9443.
53. Schöneboom, J. C., Neese, F., and Thiel, W. (2005) Toward identification of the compound I reactive intermediate in cytochrome P450 chemistry: a QM/MM study of its EPR and Mossbauer parameters, *J. Am. Chem. Soc.* **127**, 5840–5853.
54. Ogliaro, F., Cohen, S., de Visser, S., and Shaik, S. (2000) Medium polarization and hydrogen bonding effects on compound I of cytochrome P450: What kind of a radical is it really? *J. Am. Chem. Soc.* **122**, 12892–12893.
55. Ogliaro, F., de Visser, S., Cohen, S., Sharma, P. K., and Shaik, S. (2002) Searching for the second oxidant in the catalytic cycle of cytochrome P450: a theoretical investigation of the iron(III)-hydroperoxo species and its epoxidation pathways, *J. Am. Chem. Soc.* **124**, 2806–2817.
56. de Visser, S. P., Ogliaro, F., Sharma, P. K., and Shaik, S. (2002) What factors affect the regioselectivity of oxidation by cytochrome p450? A DFT study of allylic hydroxylation and double bond epoxidation in a model reaction, *J. Am. Chem. Soc.* **124**, 11809–11826.
57. de Visser, S. P., and Shaik, S. (2003) A proton-shuttle mechanism mediated by the porphyrin in benzene hydroxylation by cytochrome p450 enzymes, *J. Am. Chem. Soc.* **125**, 7413–7424.
58. de Visser, S. P., Shaik, S., Sharma, P. K., Kumar, D., and Thiel, W. (2003) Active species of horseradish peroxidase (HRP) and



- cytochrome P450: two electronic chameleons, *J. Am. Chem. Soc.* **129**, 15779–15788.
59. Ogliaro, F., de Visser, S. P., Cohen, S., Kaneti, J., and Shaik, S. (2001) The experimentally elusive oxidant of cytochrome P450: a theoretical “trapping” defining more closely the “real” species, *ChemBioChem* **11**, 848–851.
60. Schlichting, I., Berendzen, J., Chu, K., Stock, A. M., Maves, S. A., Benson, D. E., Sweet, R. M., Ringe, D., Petsko, G. A., and Sligar, S. G. (2000) The catalytic pathway of cytochrome p450cam at atomic resolution, *Science* **287**, 1615–1622.
61. Bathelt, C. M., Ridder, L., Mulholland, A. J., and Harvey, J. N. (2003) Aromatic hydroxylation by cytochrome P450: model calculations of mechanism and substituent effects, *J. Am. Chem. Soc.* **125**, 15004.
62. Bürgi, H. B., and Dunitz, J. D. (1983) From crystal statics to chemical dynamics, *Acc. Chem. Res.* **16**, 153–161.
63. Poole, J. S., Shi, X., Hadad, C. M., and Platz, M. S. (2005) Reaction of hydroxyl radical with aromatic hydrocarbons in nonaqueous solutions: A laser flash photolysis study in acetonitrile, *J. Phys. Chem. A* **109**, 2547–2551.
64. Ogliaro, F., Cohen, S., Filatov, M., Harris, N., and Shaik, S. (2000) The high-valent compound of cytochrome P450: The nature of the Fe-S bond and the role of the thiolate ligand as an internal electron donor, *Angew. Chem., Int. Ed.* **39**, 3851–3855.
65. Mico, B. A., Branchflower, R. V., Pohl, L. R., Pudzianowski, A. T., and Loew, G. H. (1982) Oxidation of carbon tetrachloride, bromotrichloromethane, and carbon tetrabromide by rat liver microsomes to electrophilic halogens, *Life Sci.* **30**, 131–137.
66. Strobel, H. W., Hodgson, A. V., and Shen, S. (1995) NADPH Cytochrome P450 Reductase and Its Structural and Functional Domains. In *Cytochrome P450: Structure, Mechanism, and Biochemistry* (Ortiz de Montellano, P. R., Ed.) 2nd ed, p 225, Plenum Press, New York.
67. Tehan, B. G., Lloyd, E. J., Wong, M. G., Pitt, W. R., Montana, J. G., Manallack, D. T., and Gancia, E. (2002) Estimation of pKa using semiempirical molecular orbital methods. Part 1: Application to phenols and carboxylic acids, *Quant. Struct.-Act. Relat.* **21**, 457–472.
68. Rietjens, I. M. C. M., and Vervoort, J. (1992) A new hypothesis for the mechanism for cytochrome P-450 dependent aerobic conversion of hexahalogenated benzenes to pentahalogenated phenols, *Chem. Res. Toxicol.* **5**, 10–19.
69. Bathelt, C. M., Ridder, L., Mulholland, A. J., and Harvey, J. N. (2004) Mechanism and structure-reactivity relationships for aromatic hydroxylation by cytochrome P450, *Org. Biomol. Chem.* **2**, 2998–3005.
70. Guallar, V., Batista, V. S., Miller, W. H., and Harris, D. L. (2002) Proton-transfer dynamics in the activation of cytochrome P450eryF, *J. Am. Chem. Soc.* **124**, 1430–1437.
71. Kamachi, T., and Yoshizawa, K. (2003) A theoretical study on the mechanism of camphor hydroxylation by compound I of cytochrome p450, *J. Am. Chem. Soc.* **125**, 4652–4661.
72. Guallar, V., and Friesner, R. A. (2004) Cytochrome P450CAM enzymatic catalysis cycle: a quantum mechanics/molecular mechanics study, *J. Am. Chem. Soc.* **126**, 8501–8508.
73. Yano, J. K., Wester, M. R., Schoch, G. A., Griffin, K. J., Stout, C. D., and Johnson, E. F. (2004) The structure of human microsomal cytochrome P450 3A4 determined by X-ray crystallography to 2.05 Å resolution, *J. Biol. Chem.* **279**, 38091–38094.

BI700365X